Chemical and photochemical behavior of ruthenium nitrosyl complexes with terpyridine ligands in aqueous media

Pablo Labra-Vázquez, Mathilde Bocé, Marine Tassé, Sonia Mallet-Ladeira, Pascal G. Lacroix, Norberto Farfan, Isabelle Malfant

ARTICLE

Chemical and photochemical behavior of Ruthenium nitrosyl complexes with terpyridine ligands in aqueous media

Received 00th January 20xx,
Accepted 00th January 20xx

DOI: 10.1039/x0xx00000x

Pablo Labra-Vázquez,[a,b] Mathilde Bocé,[a] Marine Tassé,[a] Sonia Mallet-Ladeira,[a] Pascal G. Lacroix,[a*] Norberto Farfán,[b*] Isabelle Malfant[a*]

The synthesis and behavior in water of a set of various *cis*(Cl,Cl)-[R-tpyRuCl$_2$(NO)](PF$_6$) and *trans*(Cl,Cl)-[R-tpyRuCl$_2$(NO)](PF$_6$) (R = fluorenyl, phenyl, thiophenyl; tpy = 2,2':6',2"-terpyridine) is presented. In any case, one chlorido ligand is substituted by a hydroxo ligand and the final species arise as a single *trans*(NO,OH) isomer, whatever the nature of the starting *cis*/*trans*(Cl,Cl) complexes. Six X-ray crystal structures are presented for the *cis*(Cl,Cl)-[thiophenyl-tpyRuCl$_2$(NO)](PF$_6$) (*cis*-**3a**), *trans*(Cl,Cl)-[thiophenyl-tpyRuCl$_2$(NO)](PF$_6$) (*trans*-**3a**), *trans*(NO,OH)-[phenyl-tpyRu(Cl)(OH)(NO)](PF$_6$) (**4a**), *trans*(NO,OH)-[thiophenyl-tpyRu(Cl)(OH)(NO)](PF$_6$) (**4b**), *trans*(NO,OEt)-[phenyl-tpyRu(Cl)(OEt)(NO)](PF$_6$) (**5a**), and *trans*(NO,OH)-[phenyl-tpyRu(Cl)(OEt)(NO)](PF$_6$) (**5b**) compounds. The different *cis*/*trans*(Cl,Cl) complexes exhibit an intense low-lying transition in the λ = 330 – 390 nm range, which appears slightly blue-shifted after Cl $\rightarrow$ OH substitution. In water, both *cis*/*trans*(Cl,Cl) isomers lead to a conversion to a single *trans*(NO,OH) isomers in which one chlorido- is replaced by one hydroxo- ligand, which avoid tedious separation workout. The water stable *trans*(NO,OH)-species all release NO with quantum yields of 0.010 to 0.075 under irradiation at 365 nm. The properties are discussed with computational supports performed within the framework of the Density Functional Theory.

INTRODUCTION

Ruthenium nitrosyl (Ru-NO) complexes are a class of intriguing photo-reactive species, with either metal nitrosyl to metal isonitrosyl ([metal-NO] $\leftrightarrow$ [metal-ON]) switching properties[1] or nitric oxide (NO$^{\cdot}$) releasing capabilities.[2,3] As switching materials, they have led to a nearly 100 % solid state isomerization in [RuCl(NO)py$_4$](PF$_6$)$_2$·1/2H$_2$O (py = pyridine),[4] with high potential applications in data storage, holography and real-time optical technologies.[5-8] As NO$^{\cdot}$ donors, they have been attracting a growing research activity in relation to the recognition of the numerous biological functions of NO$^{\cdot}$ (*e.g.* blood pressure regulation, stimulation of immune response, neurotransmission and cytotoxic activity in tumor cells).[9,10] Due to the increasing number of papers dedicated to the NO$^{\cdot}$ delivery in the current literature,[11] and although our initial interest for ruthenium-nitrosyl complexes was centered on the concept of "molecular switch", we became gradually encouraged to consider these materials as NO$^{\cdot}$ donors as well. Indeed, an intense research activity is dedicated to NO$^{\cdot}$ donors capable to release NO$^{\cdot}$ locally and quantitatively.[12,13] Among them, Ru-NO complexes appear especially promising in relation to their usually low toxicity, good chemical stability and their capability to release NO$^{\cdot}$ under irradiation, exclusively,[2,14,15] taking advantage of the noninvasive character and precise control of light.

Our first investigations of NO$^{\cdot}$ release were undertaken on different sets of *cis*(Cl,Cl)[R-tpyRuCl$_2$(NO)](PF$_6$) and *trans*(Cl,Cl)[R-tpyRuCl$_2$(NO)](PF$_6$) compounds in which R-tpy stands for a 4'R-2,2':6',2"-terpyridine (Scheme 1). In these species, various R substituents were introduced, such as a fluorenyl (**c** in Scheme 1),[16] or a set of donor/acceptor-substituted phenyls[17] used to modulate the "push-pull" charge transfer character towards the highly withdrawing Ru-NO unit, in an attempt to optimize the two-photon absorption (TPA) response of the species. Indeed, the use of the TPA technics, has become a powerful tool in life sciences by virtue of its low damage effects, high spatial selectivity and deep penetration into biological tissues.[18,19] Therefore, the quantification of the TPA response of these compounds is an important parameter to determine. Due to a lack of fluorescence, the properties were evaluated by the Z-scan technics,[20] in which the standard conditions require the use of organic solvents, as organics provide the largely dominant class of optical molecular

[a] *Laboratoire de Chimie de Coordination du CNRS, 205 route de Narbonne, F-31077, Toulouse, France.*
[b] *Facultad de Química, Departamento de Química Orgánica, Universidad Nacional Autónoma de México, Ciudad Universitaria, 04510 Ciudad de México, México.*

Electronic Supplementary Information (ESI) available: [details of any supplementary information available should be included here]. See DOI: 10.1039/x0xx00000x

materials. Indeed, recording TPA data in water by Z-scan is not well documented and no fully relevant for our complexes of TPA cross-sections in the 100 – 200 GM range,[21] due to their modest solubility and to the significant contribution of the solvent to the TPA signal.[22-25] Therefore, and for homogeneity reasons, we have conducted the entire physicochemical investigations in acetonitrile, which was found to be a better solvent. However, and at a more fundamental level, switching from optical materials to biological materials implies to investigate the chemical and physical properties of the active species in aqueous media. Along this line, we have recently observed that low concentrations of "terpyridine Ru-NO" complexes (10^{-6} mol.L^{-1}) could make bacteria (*Staphylococcus epidermidis*) 100 times more sensitive to methicillin.[26] Additionally, we have observed that the nature of the active complex in aqueous solution was not [R-tpyRuCl_2(NO)]$^+$ but [R-tpyRuCl(OH)(NO)]$^+$, in which a chlorido ligand has surprisingly been replaced by an hydroxo ligand.

In the present contribution, and following this first observation, we wish to report on the complete chemical behavior of [R-tpyRuCl_2(NO)]$^+$ complexes in water, and on their photorelease capabilities compared with those previously observed in organic media. The selected complexes for this investigation are shown in Scheme 1. The synthesis of the compounds is reported first, with their characterizations, and crystal structures. A computational analysis is reported to provide theoretical supports to the experimental data, within the framework of the density functional theory (DFT).

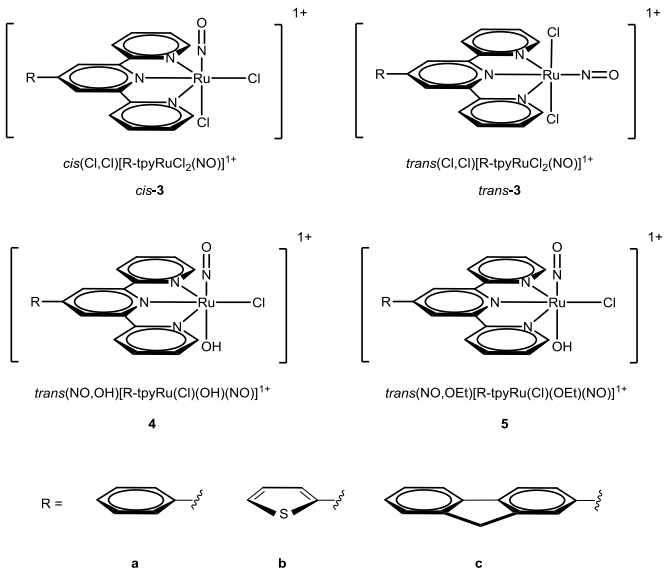

Scheme 1. Ruthenium nitrosyl complexes under investigation

RESULTS AND DISCUSSION

Synthesis and characterization

The synthesis of the target complexes was carried out in 3 steps from the 4'-substituted terpyridyl ligands **1a**-**c** (Scheme 2), which were accessed through the Kröhnke pyridine synthesis.[27,28] The first step involved the introduction of the Ru^{III} metal center by treatment of ethanolic solutions of the ligands with $RuCl_3 \cdot xH_2O$, yielding complexes **2a**-**c**. This reaction proceeded with moderate yields due to the concomitant formation of the homoleptic species $[Ru^{III}(R\text{-tpy})_2]^{2+}$, which was identified as an important by-product in this reaction.

After purification, warm solutions of **2a**-**c** in DMF were bubbled with nitric oxide for 3-5 hours yielding ruthenium nitrosyls **3a**-**c** in high yields by ligand exchange of one chlorido ligand for NO^+. By these means we obtained crude materials composed mainly by the *cis*(Cl,Cl)-[Ru^{II}(**1a**-**c**)Cl_2(NO)](Cl) (*cis*-**3a**-**c**) and *trans*(Cl,Cl)-[Ru^{II}(**1a**-**c**)Cl_2(NO)](Cl) (*cis*-**3a**-**c**) isomers, as evidenced by ^{1}H-NMR analysis of these mixtures (See SI Figures S1-S3). Although our primary objective lied on studying water-stable complexes **4a**-**c**, we were able to isolate analytical samples of previously unknown *cis*-**3b** and *trans*-**3b** as their PF_6 salts after HPLC purification followed by metathesis with NH_4PF_6.

Finally, the target *trans*(NO,OH)-[Ru^{II}(**1a**-**c**)(NO)(OH)Cl]((PF_6) complexes (**4a**-**c**) were obtained from crude samples of **3a-c**, which leaded to these compounds after refluxing in water overnight, with a notorious change in the reaction color from orange to yellow. In several attempts, after concentrating the reaction mixtures *in vacuo*, pure samples of these complexes were obtained in high yields after treatment with NH_4PF_6. Nonetheless, in some cases, especially for **4b**, further chromatographic workup was necessary.

Moreover, we found that the hydroxo ligand in the *trans*(NO,OH) complexes **4a-c** could be readily replaced by an ethanolate during a short thermal treatment with ethanol. This solventolysis produced the *trans*(NO,OEt) complexes **5a**-**b** in excellent yields. By following the UV-Vis photokinetics of these complexes in water, we found that the ligand exchange process is not reversible at room temperature, thus we were further interested in investigating if these complexes retained $NO^{\cdot}$ release when irradiated in water. It was interesting to find that while the OH $\rightarrow$ OEt replacement takes place easily on crude samples of compounds **4a**-**c**, no product is observed when attempting the ligand exchange reaction to convert directly **3a** to **5a**, even after long reaction times. This observation is in disagreement with the fact that chloride is usually regarded as a better leaving group than hydroxide.

Unambiguous assignment of the ^{1}H and ^{13}C spectra was performed aided by ^{1}H, ^{13}C monodimensional NMR techniques as well as by 2D heteronuclear HMQC/HMBC (^{1}H-^{13}C) and homonuclear (^{1}H-^{1}H) COSY/NOESY experiments. In every case, two spin systems were readily identified in the COSY experiments, one belonging to the 2,2':6',2''-terpyridyl core whose protons appear as very deshielded multiplets due to long-range through-bond spin-state transmission within the aromatic system including hydrogens H-1 to H-4, and a second spin system usually upfielded, belonging to the substituent

attached to the terpyridyl core (Phenyl, thien-2-yl, 9H-fluorenyl).

As illustrated in Figure 1 along the **b** series, the Cl → OH → OEt ligand exchanges can be readily traced by means of ^{1}H-NMR, where most of the signals from the 2,2':6',2''-terpyrydyl core are upfielded as the σ-withdrawing chlorido ligand is replaced by -OH and furthermore by -OEt. Nevertheless, such trend does not match exactly the Hammett constants for these ligands: Cl (σp = 0.227), OEt (σp = -0.24) and OH (σp = -0.37),[29] even though it explains the upfield shift when going from -Cl to -OH, it does not explain the upfield shift from -OH to -OEt. Nonetheless, the overall shielding of the hydrogens within the terpyridyl ligands suggests that the electron density of the Ru-NO submolecular fragment decreases in the order OEt > OH > Cl, thus the Cl to OR ligand exchange decreases Ru-NO π-backdonation in the opposite order (Cl > OH > OEt), with an associated reduction of the N-O bond order. As discussed below (*vide infra*), these preliminary observations correlated well with the results obtained by using infrared spectroscopy, and X-Ray diffraction experiments.

X-Ray Diffraction Studies

Crystals of *cis*-**3b**, *trans*-**3b**, **4a**-**b** and **5a**-**b** suitable for X-ray crystallographic analyses were grown by slow diffusion of diethyl ether into saturated solutions of the analytes in acetonitrile at room temperature. The molecular structures and main crystallographic data for these complexes are presented in Figure 2, and Table 1, respectively.

With the exception of *trans*-**3b**, for which two crystallographically independent, yet geometrically closely-related, complexes are found in its asymmetric unit, all the other compounds crystallize with a single complex per asymmetric unit. Also, with the exception of compounds **5a**-**b**, all crystallize as acetonitrile solvates, with the solvent molecule in close contact with the electron-deficient hydrogen H-1; nevertheless, despite short C(1)-H(1)…N$_{(acetonitrile)}$ distances are observed (2.4 – 2.8 Å), the geometries lie considerably far from linear (with 98–140° D-H…A angles) to postulate a nonclassical hydrogen bonding interaction.

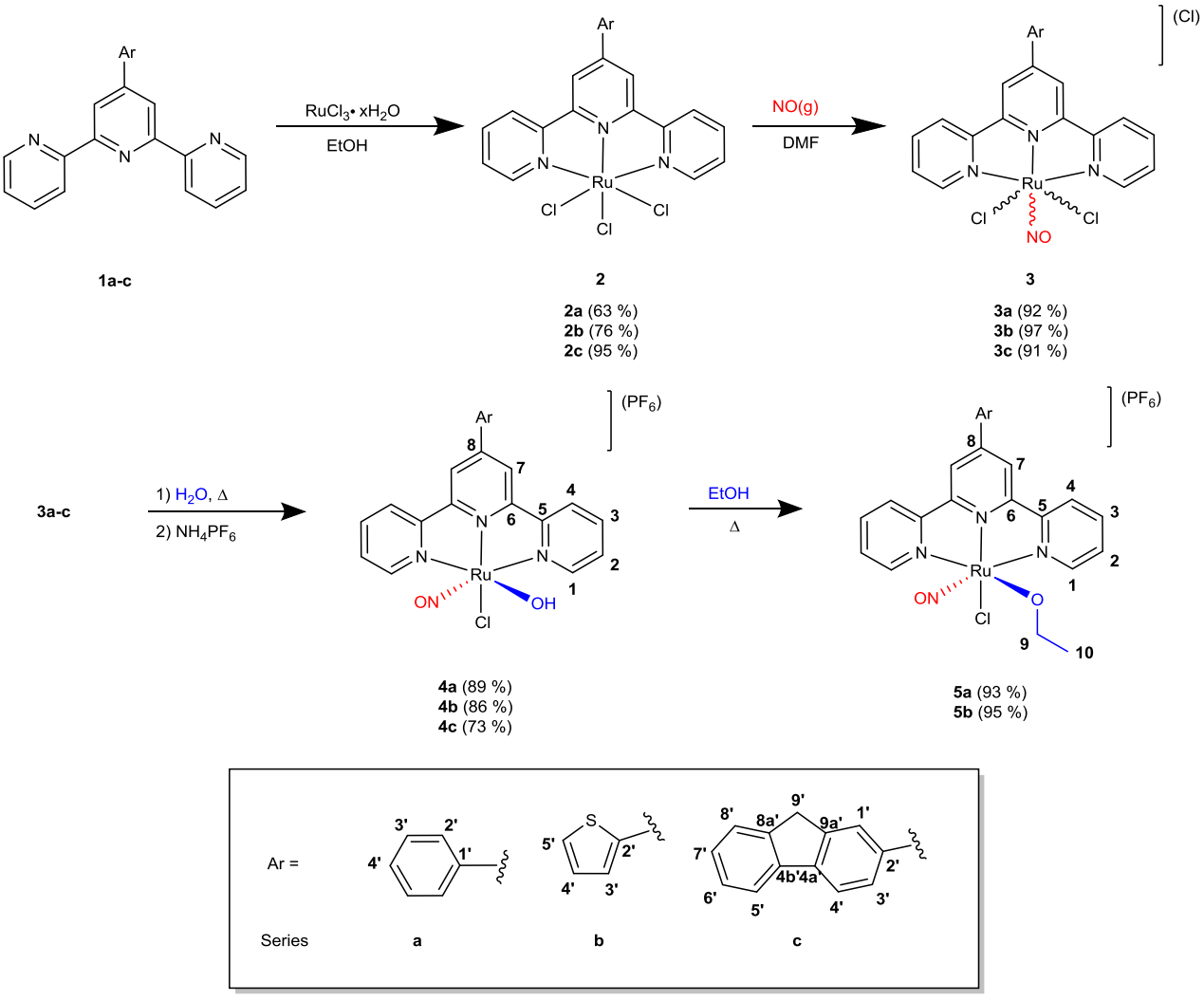

Scheme 2. Synthesis and numbering for complexes **4a-c** and **5a-b**.

ARTICLE

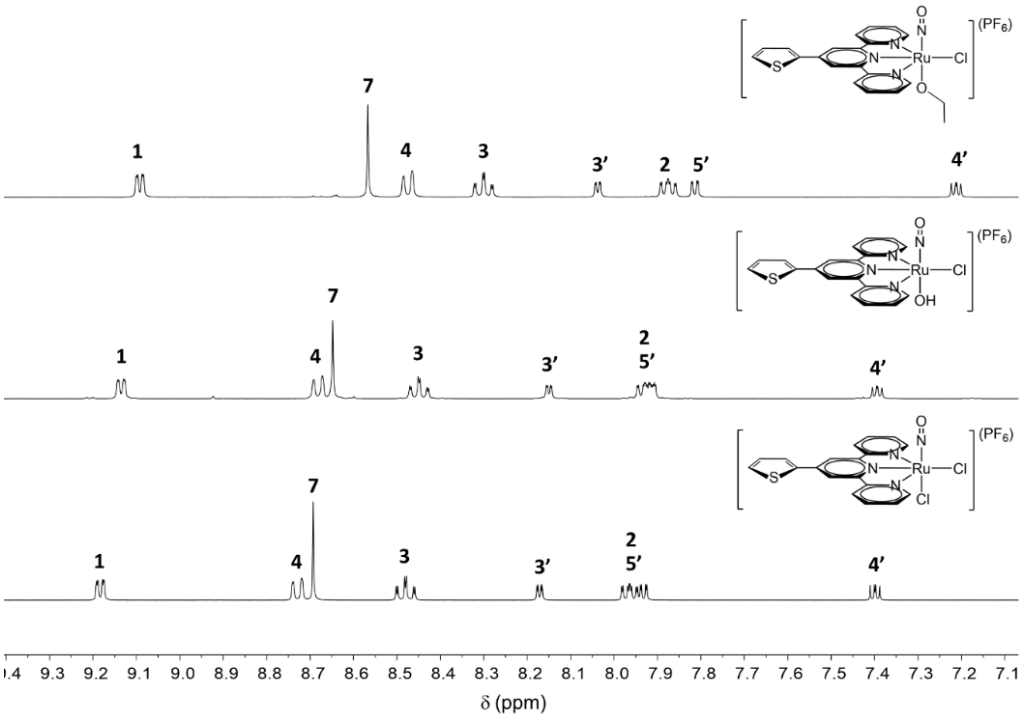

Figure 1. ^{1}H-NMR spectra of selected complexes *cis*-**3b** (bottom), **4b** (center) and **5b** (top) [400 MHz, CD_3CN]. See Scheme 2 for the numbering.

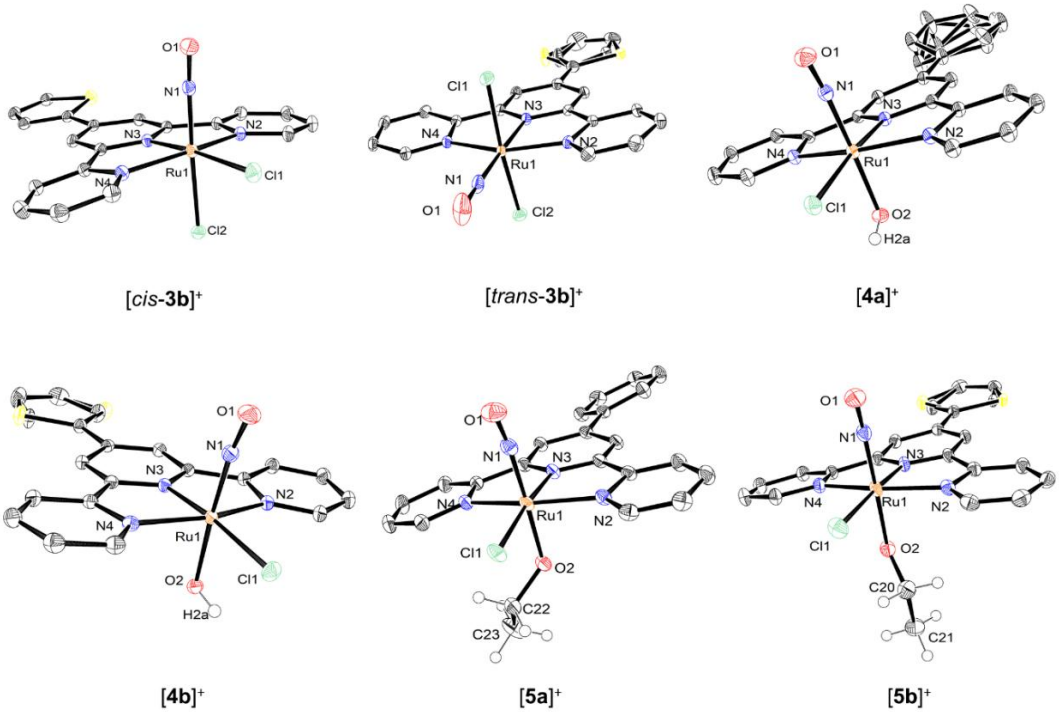

Figure 2. Molecular structure of complexes *cis*-**3b**, *trans*-**3b**, **4a-b** and **5a-b**. Only selected hydrogen atoms are shown for clarity. Thermal ellipsoids are drawn at 50 % probability for every atom other than hydrogen.

Selected bond lengths and angles are gathered in Table 2, for the coordination spheres of the 6 reported structures. Similar to other ruthenium nitrosyls with $\{Ru(NO)\}^6$ Enemark-Feltham notation[30] such as $[RuCl_5NO]^{2+}$ and $[RuNO(NH_3)_5]^{3+}$, the present

Table 1 Crystal Structure and Refinement Data.

	cis-**3b**	*trans*-**3b**	**4a**	**4b**	**5a**	**5b**
empirical formula	$C_{19}H_{13}Cl_2N_4ORuS$ PF_6, CH_3CN	$C_{19}H_{13}Cl_2N_4ORuS$ PF_6, CH_3CN, 0.25(H_2O)	$C_{21}H_{16}ClN_4O_2Ru$ PF_6, CH_3CN	$C_{19}H_{14}ClN_4O2RuS$ PF_6, CH_3CN	$C_{23}H_{20}Cl\ N_4O_2Ru$ PF_6	$C_{21}H_{18}ClN_4O_2RuS$, PF_6
temperature (K)	115(2)	113(2)	110(2)	110 (2)	100(2)	100 (2)
crystal system	Monoclinic	Triclinic	Monoclinic	Monoclinic	Triclinic	Triclinic
space group	$P2_1/n$	$P\ \bar{1}$	$C2/c$	$C2/c$	$P\ \bar{1}$	$P\ \bar{1}$
a (Å)	16.243(5)	13.3561(5)	22.9917(8)	22.9490(8)	11.012(2)	7.6895(4)
b (Å)	7.354(2)	14.1266(5)	17.2990(6)	16.5682(7)	11.092(2)	10.6774(6)
c (Å)	21.148(8)	14.3152(5)	14.1597(5)	14.2190(6)	11.139(2)	15.5498(9)
α (deg)	90	104.9716(16)	90	90	75.537(7)	80.941(2)
β (deg)	93.548(10)	96.3207(16)	114.003(2)	112.0015(12)	79.228(7)	85.288(2)
γ (deg)	90	97.3251(17)	90	90	70.732(7)	69.984(2)
volume (Å)^3	2521.3(14)	2558.96(16)	5144.8(3)	5012.7(3)	1235.5(4)	1184.07(12)
Z	4	4	8	8	2	2
Density (g.cm^{-3})	1.853	1.836	1.753	1.815	1.790	1.88
Crystal size (mm)	0.6 × 0.32 × 0.2	0.15 × 0.12 × 0.05	0.2 × 0.2 × 0.2	0.18 × 0.15 × 0.15	0.2 × 0.06 × 0.04	0.13 × 0.10 × 0.
θ range (deg)	2.93-34.97	1.49-28.31	3.78-37.83	1.56-30.53	1.90-29.57	1.33-28.40
reflns collected/ unique	129329/11066	61829/12669	105871/13630	77701/7610	47404/6911	68687/5944
final R indices	R_1 = 0.0305	R_1 = 0.0352	R_1 = 0.0252	R_1 = 0.0214	R_1 = 0.0341	R_1 = 0.0315
[I >2σ(I)]	wR_2 = 0.0665	wR_2 = 0.0469	wR_2 = 0.0627	wR_2 = 0.0361	wR_2 = 0.0801	wR_2 = 0.0429
R indices	R_1 = 0.0413	R_1 = 0.0396	R_1 = 0.0310	R_1 = 0.0271	R_1 = 0.0460	R_1 = 0.0369
(all data)	wR_2 = 0.0715	wR_2 = 0.0622	wR_2 = 0.0674	wR_2 = 0.2002	wR_2 = 0.0863	wR_2 = 0.0490

complexes possess Ru(1)-N(1)-O(1) angles close to 180 °, however with a tendency for reduced angles in the complexes in which -Cl is replaced by -OH and -OEt. (**4a**-**c**, **5a**-**b**). This observation suggests that the Ru-NO π-backbonding is enhanced in the later systems. Accordingly, when comparing a series with the same terpyridyl ligand, e.g. **cis**-**3b**, **4b** and **5b**, the N(1)-O(1) bond distance follows **5b** > **4b** > *cis*-**3b**. Both reduced angles and enhanced bond lengths are consistent with a decreasing N-O bond order. Furthermore, these observations correlate well with previous discussions on the NMR spectra and with the infrared spectroscopy of these complexes as discussed below.

Some of the most intriguing supramolecular interactions within the crystal packing of this family of complexes are here represented with those observed for the *cis*-**3b** and *trans*-**3b** isomers. As exemplified in Figure 3, the crystal packing of these complexes which possess electron-rich thiophene rings, showed clear examples of offset π-stacking,[31,32] formed by the alignment of pairs of complexes in a displaced anti-parallel fashion, putting alternating electron-deficient (central or lateral pyridine) and electron-rich (thiophene) rings close to each other. Given the complementarity of the interaction and the short distances between the pyridine-thiophene rings centroids (*e.g.* 3.472 Å for *cis*-**3b**), this interaction is likely one of the main driving forces for the crystallization process, as the resulting arrangement contributes to reduce electrostatic repulsion along the crystal lattice.

As depicted in Figure 3b, the scenario is different for the *trans*-**3b** isomer, which features an unprecedented short distance (2.566 Å) between the oxygen of two neighboring nitrosyls. Given the *quasi* linearity of the Ru-NO bond, these oxygen atoms are expected to be positively charged, making this close contact rather unlikely to occur. Nonetheless, further analysis of the crystal structure suggests that this arrangement is stabilized by the closeness of two PF_6^- counterions at the sides of the nitrosyls as well as by a complementary offset π-stacking interaction with an intercentroid distance of 3.577 Å, in this case involving the thiophene ring and one of the lateral rings of a neighboring complex.

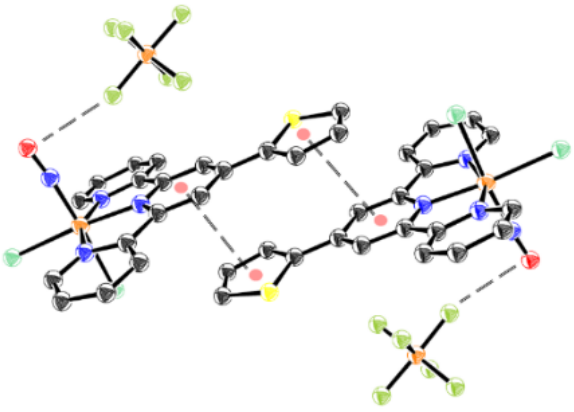

(a)

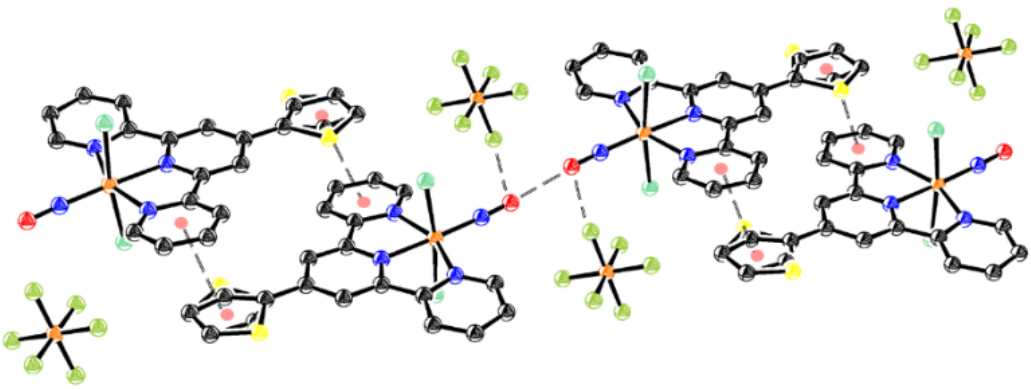

(b)

Figure 3 Supramolecular interactions within the crystal packing of (a) *cis*-**3b** and (b) *trans*-**3b**. Hydrogen atoms and solvent molecules are omitted for clarity.

Table 2 Selected bond lengths and angles.

Selected bonds (Å)	*cis*-**3b**	*trans*-**3b**		**4a**	**4b**	**4c**[a]	**5a**	**5b**
		mol 1	mol 2					
Ru(1)-N(1)	1.7617(14)	1.777(2)	1.754(2)	1.7632(9)	1.7626(12)	1.761(3)	1.771(2)	1.759(2)
Ru(1)-N(2)	2.0863(14)	2.075(2)	2.069(2)	2.0881(8)	2.0920(11)	2.086(3)	2.097(2)	2.085(2)
Ru(1)-N(3)	1.9869(13)	1.999(2)	2.005(2)	1.9756(8)	1.9766(10)	1.981(3)	1.9824(19)	1.983(2)
Ru(1)-N(4)	2.0930(13)	2.088(2)	2.069(2)	2.0849(8)	2.0891(11)	2.081(3)	2.088(2)	2.085(2)
Ru(1)-Cl(1)	2.3934(7)	2.3312(7)	2.3666(7)	2.3890(2)	2.3889(3)	2.4020(8)	2.4083(7)	2.3949(7)
Ru(1)-Cl(2)	2.3501(7)	2.3718(7)	2.3459(7)	-	-	-	-	-
Ru(1)-O(2)	-	-	-	1.9499(8)	1.9532(9)	1.950(2)	1.9504(18)	1.9424(17)
N(1)-O(1)	1.1380(18)	1.126(3)	1.125(3)	1.1469(12)	1.1494(16)	1.147(4)	1.146(3)	1.154(3)
Selected angles (deg)								
N(1)–Ru(1)–N(3)	96.83(5)	175.59(10)	176.71(11)	98.56(4)	98.92(5)	97.43(12)	97.12(9)	97.25(9)
N(3)–Ru(1)–N(4)	79.42(5)	78.26(9)	78.84(9)	79.76(3)	79.83(4)	79.51(11)	79.63(8)	79.71(8)
Cl(1)–Ru(1)–Cl(2)	87.766(17)	174.80(3)	172.35(3)	-	-	-	-	-
Cl(1)–Ru(1)–N(1)	88.55(4)	95.67(8)	91.07(7)	87.67(3)	87.48(4)	88.47(9)	87.19(7)	87.08(7)
N(1)-Ru(1)-O(2)	-	-	-	176.41(3)	176.02(5)	176.27(11)	178.04(8)	177.57(9)
Ru(1)–N(1)–O(1)	174.93(13)	172.9(3)	-	170.57(8)	170.47(11)	173.8(3)	171.97(19)	170.5(2)

[a] Data for **4c** are from Ref. 26

Infrared spectroscopy

All of the ruthenium nitrosyl complexes were studied by means of FT-IR (ATR) spectroscopy. Of particular interest to the current work were the energies for the νNO band, as it holds firsthand information on the electron density present on the nitrosyl ligands and hence on the intramolecular charge transfer within the complexes. The experimental data are presented in Table 3. The values fall in the 1814 – 1913 cm^{-1} range in any case, in agreement with linear or *quasi* linear Ru-NO bonds as those observed in the SXRD experiments (*vide supra*). The most valuable information comes from comparing a series with the same terpyridyl ligand. For example, the energy of the νNO band decreases in the order: *cis*-**3b** > *trans*-**3b** > **4b** > **5b** and, accordingly, the degree of π-backdonation to the NO ligand should decrease in the opposite order. Indeed, this process brings electron density into π^* antibonding orbitals, thus reducing the bond order and hence the νNO frequency. These observations are in full agreement with the previously discussed NMR and structural data (*vide supra*).

The analyses of νNO frequency provides an additional and important information on the stability of ruthenium nitrosyl complexes. Indeed, some of our [tpyRuNO] species were reported to possess a high sensitivity to water, according to the non-redox following reaction:

$$Ru^{II}(NO)^{+} + 3\ H_2O \rightleftharpoons Ru^{II}(NO_2)^{-} + 2\ H_3O^{+} \qquad (1)$$

This deleterious reaction is especially observed when the chlorido ligands are replaced by a bipiridine.[21c] νNO frequencies higher than 1920 cm^{-1} indicate that the degree of the positive charge residue on NO is high, which reflects the tendency for NO to be subjected to nucleophilic attacks, thus leading to the formation of $Ru^{II}(NO_2)^{-}$ depicted in equation (1). By contrast, νNO frequencies equal or lower than 1900 cm^{-1} indicate a good stability in aqueous media.[33,34] This later case is that observed here (1814 $cm^{-1} \leq$ νNO $\leq$ 1913 cm^{-1}), which indicates that the RuNO units are stable in water.

The chlorido to hydroxo ligand exchange

Examples of ligand exchange reactions on ruthenium nitrosyl complexes with the general formula $[(R\text{-tpy})RuCl_2(NO)]^{+}$ where R-tpy is any functionalized 2,2':6',2''-terpyridine ligand, remain very scarce up to date. To the best of our knowledge, only two reports on such reactions have been published, one by Nagao,[35] and one recent report by our group.[26] This may in turn be due to the fact that, despite the synthetic route employed, the synthesis of the starting materials invariantly yields complex mixtures containing both the *cis*(Cl,Cl)- and *trans*(Cl,Cl)-$[(R\text{-tpy})RuCl_2(NO)]^{+}$ isomers, as well as varying amounts of homoleptic $[Ru(R\text{-tpy})_2]^{2+}$ species. The purification of these compounds typically requires costly and tedious HPLC procedures,[17] thus precluding most further synthetic derivatizations. Nevertheless, Nagao *et al*. showed that *trans*(Cl,Cl)-$[Ru(tpy)Cl_2(NO)](PF_6)$ undergoes ligand exchange reactions either with water or $NaNO_2$ in methanol to yield *trans*(NO,OH)-$[Ru(tpy)(NO)(OH)(Cl)](PF_6)$ and *trans*(NO,OCH_3)-$[Ru(tpy)(NO)(OCH_3)(Cl)](PF_6)$, respectively, in low to moderate yields. Our synthetic approach was significantly different, as we encountered several problems when trying to perform the ligand exchange in water from complexes containing the PF_6^- counterion as these species were notably less soluble in water when compared to their Cl^- salts. Also, our protocol involved the use of crude starting materials containing only minimum amounts (typically below 3 %) of the undesired homoleptic species, thus greatly simplifying the purification of the final products.

The observation of the replacement of one chlorido ligand by a hydroxo ligand in any case is further supported by a theoretical investigation. Indeed, the Gibbs free energies (ΔG°) were computed for the following equations:

$$[cis\text{-}\mathbf{3a}]^{+} + OH^{-} \rightarrow [trans(NO,OH)\text{-}\mathbf{4a}]^{+} + Cl^{-} \qquad (2)$$
$$[cis\text{-}\mathbf{3b}]^{+} + OH^{-} \rightarrow [trans(NO,OH)\text{-}\mathbf{4b}]^{+} + Cl^{-} \qquad (3)$$
$$[cis\text{-}\mathbf{3c}]^{+} + OH^{-} \rightarrow [trans(NO,OH)\text{-}\mathbf{4c}]^{+} + Cl^{-} \qquad (4)$$

The resulting ΔG° values of -64.8 kcal mol^{-1}, -64.9 kcal mol^{-1}, and -61.0 kcal mol^{-1} for equation (2), (3), and (4), respectively, indicate a clear tendency for the chlorido to hydroxo substitution. No further investigation was undertaken to clarify the details of the formation of the Ru-OH band. Nevertheless, and as the pH of the solution is in the 5-7 range, the substitution likely proceeds through a concerted mechanism, thus avoiding the formation of unstable high energy $[Ru(Cl)(H_2O)(NO)]$ intermediates.

The most striking feature about the chlorido to hydroxo ligand exchange is that, while three different isomers could be expected (Scheme 3), ^{1}H-NMR analysis of the crude products evidenced the formation of a single final isomer, *trans*(NO,OH)-$[Ru(R\text{-tpy})(Cl)(OH)(NO)](PF_6)$ (**4a**-**c**), even though mixtures of both *cis*(Cl,Cl) and *trans*(Cl,Cl)-$[Ru(R\text{-tpy})Cl_2(NO)](Cl)$ isomers are used as starting materials.

Table 3. DFT Computed νNO frequencies (in cm^{-1}) compared with experimental data, for the ruthenium-nitrosyl derivatives.

	cis-**3a**	*trans*-**3a**	*cis*-**3b**	*trans*-**3b**	**4a**	**4b**	**5a**	**5b**
Computation	2007	2015	2005	2012	1966	1964	1953	1952
Experimental	1911[a] 1897[a]	1907[a]	1887	1913	1834	1857	1814	1835

[a] data from Ref. 17

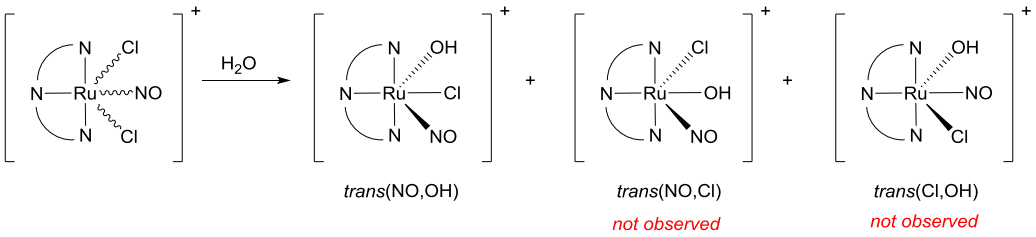

Scheme 3. Potential outcome for the Cl to OH ligand exchange.

Table 4 Relative Gibbs free energies (G°) for the three isomers of $[R\text{-tpyRu(Cl)(NO)(OH)}]^+$ computed in water, with ν_{NO} frequencies.

R	isomer	relative energies[a] (in kcal/mol)
Fluorene **4c**	*trans*(Cl,NO)	+ 9.8
	trans(Cl,OH)	+ 5.7
	trans(NO,OH)	0
DMAphen	*trans*(Cl,NO)	+ 9.6
	trans(Cl,OH)	+ 5.7
	trans(NO,OH)	0
NO_2phen	*trans*(Cl,NO)	+ 9.3
	trans(Cl,OH)	+ 5.9
	trans(NO,OH)	0

[a] for each (R =fluorene, DMAphen and NO_2phen) containing complexes, the reference energy (G° = 0) is that of the most stable isomer.

The Gibbs energies were computed for the three different isomers, to provide a theoretical support to this observation. In order to determine if the relative stabilities are influenced by the electronic capabilites of the R-tpy terpyridine fragments, the computations were performed on complexes in which R is either a strongly electron rich dimethylaminophenyl (DMAphen) substituent or a strongly electron withdrawing nitrophenyl (NO_2phen) substituent. The results are gathered in Table 4. Clearly, the data reveal that the relative energies of the isomers do not depend on the donor/acceptor character of the R substituent. The computation extended to the case of fluorenylterpyridine containing complex **4c** confirm that the *trans*(NO,OH) isomer is invariably the most stable species in any case. Along this line, the (Cl → OH) substitution reaction occurring in water could appear as an elegant mean of avoiding the usually tedious workout required for the separation of the starting *trans*(Cl,Cl) and *cis*(Cl,Cl) isomers mixture obtained in the initial synthesis of the $[(terpyridine)RuCl_2(NO)]^+$ species.

As exemplified in Figure 4 with *cis*-**3b** and *trans*-**3b**, further evidence for the formation of a single isomer during the chlorido to hydroxo ligand exchange from compounds **3a-c** was found by independently following the spectral evolution of pure samples of both *cis*(Cl,Cl) and *trans*(Cl,Cl)-$[Ru(R\text{-tpy})Cl_2(NO)](PF_6)$ complexes in water (details for additional experiments can be found in the ESI, Figure S29).

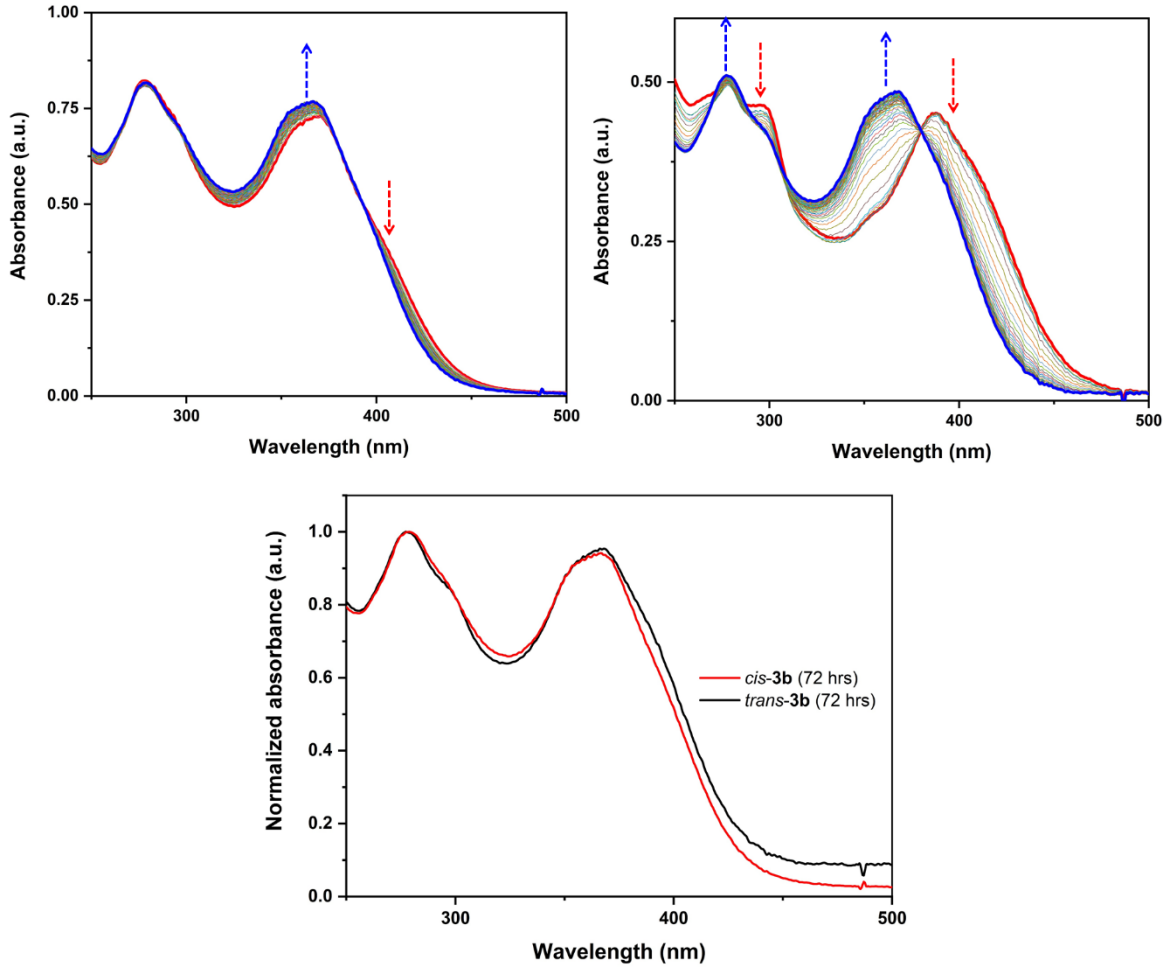

Figure 4. Spectral evolution in water (0.5% of DMSO) for *cis*-**3b** (top, left) and *trans*-**3b** (top, right) at room temperature ($4x10^{-5}$ M, 72 hrs). A comparison between the end points for both kinetics is shown in the bottom.

A clean conversion to a single isomer can thus be inferred from the presence of the same isosbestic point at λ = 380 nm for both isomers, and by the fact that the end point of both kinetics yielded superimposable spectra.

UV-visible spectroscopy

Mapping of the electronic structure of these complexes was conducted by means of UV-Vis spectroscopy in acetonitrile (Figure 5). The results can be summarized as follows: (i) all the ruthenium nitrosyl complexes feature a strong band (ε > 20,000 $M^{-1}cm^{-1}$) located around λ = 300 nm, which accounts for a local $\pi-\pi*$ excitations within the 4'-substituted 2,2':6',2''-terpyridyl ligand, and (ii) low-lying and less intense transitions are located around λ = 400 nm, accounting for strong intramolecular charge transfers towards the nitrosyl substituents. These electronic features are fully consistent with our previous investigations of terpyridine-based RuNO complexes.[16,17,36]

The UV-visible data (λmax and ε) for the low-lying transitions of the complexes are gathered in Table 5 with those of the *cis*-**3a** and *trans*-**3a** species, previously investigated. The comparison leads to the following conclusions: (i) there is a slight bathochromic shift in the *trans*(Cl,Cl) isomers with respect to the *cis*(Cl,Cl) isomers within the **3a-b** series related to the better overlap, and hence stronger push-pull character towards the nitrosyl substituent when it lies in the same plane than the terpyridyl ligand in the complexes; (ii) there is a global red shift of about 20 nm on going from the phenyl to the thiophenyl substituents, in relation to an increased donating capability and better planarity within the thiophenyl-terpyridine unit. ~~As reflected by the Hammett constant of the thiophenyl (σp = -0.43) markedly lower than that of phenyl (σp = -0.18);~~[25] (iii) along a phenyl (**a**) or thiophenyl (**b**) series having the same terpyridyl ligand and nitrosyl in axial (*cis*) position, the energy for the low-lying transitions follows: **5** ≈ **4** > *cis*-**3**. To check out the origin of these various effects, the details of the TD-DFT computed transitions are provided in Table 6.

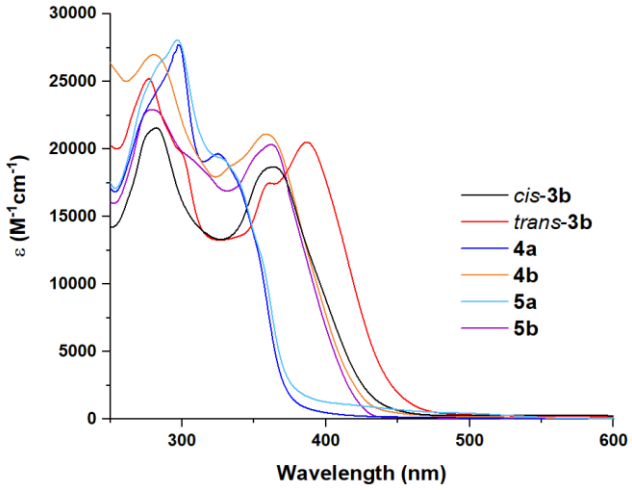

Figure 5. UV-visible spectra in acetonitrile for compounds *cis*-**3b,** *trans*-**3b, 4a-b** and **5a-b**

Table 5 UV-visible low-lying transition recorded in acetonitrile for the ruthenium-nitrosyl complexes and related TD-DFT-computed data

	UV-visible		TD-DFT	
	λ_{max} (nm)	ε (mol^{-1}.L cm^{-1})	λ_{max} (nm)	f
cis-**3a**	330[a]	17 400[a]	299	0.528
trans-**3a**	350[a]	18 800[a]	312	0.363
cis-**3b**	363	18 700	335	0.657
trans-**3b**	387	20 500	348	0.607
	361	17 500	327	0.138
4a	325	19 700	292	0.469
4b	358	21 100	327	0.751
4c	380	23 000	343	0.962
5a	328	19 300	291	0.194
			289	0.250
5b	362	20 350	327	0.706

[a] Ref. 17

The data gathered in Table 6 reveal that low-energy transitions always possess a dominant HOMO → LUMO contribution in the case of complexes **3** and **4**, in which the coordination spheres correspond to tpyRuCl$_2$(NO) and tpyRu(Cl)(OH)(NO), respectively. More precisely, the examination of the orbitals (Figure 6) shows that the electronic effect associated to these transitions is that of a charge transfer from the electron rich substituent of the terpyridine ligand to the withdrawing RuNO fragment. Using a thiophenyl substituent (**b**) clearly increases the energy of the HOMO levels by about 0.4 eV versus that of the phenyl substituent (**a**), which leads to redshifted push-pull transitions (Table 5). These features are in agreement with our previous reports on terpyridine-RuCl$_2$(NO) species, where the energy of the occupied level, and hence that of the charge transfer transition towards RuNO, is related to the donor/acceptor character of the substituent present on the terpyridine.[16a,17,36] Interestingly, the case of complexes **5**, where the hydroxo ligand is replaced by an ethanolato ligand, appears different. Contrary to the situation encountered with OH ligand, the *p* orbital of the oxygen atom of OEt (orbital 117 (HOMO) in **5a** and orbital 117 (HOMO-1) in **5b**) is involved in the charge transfer. Furthermore, its contribution becomes dominant in **5a** (50 % of the effect in transition 1 → 12, in Table 6). The difference on going from **4a** (OH) to **5a** (OEt) can tentatively be related to structural effects, and is depicted in Figure 7. Due to hydrogen bonding, the Cl-Ru-O-H torsion angle is equal to 0 degree in **4a**. This implies that orbital 108 (HOMO-1, *p* orbital of the oxygen of the hydroxo) is orthogonal to orbital 112 (LUMO+2, RuNO fragment with a strong contribution of d_{xz}). In other words, orbital 108 adds no contribution to the 109 → 110 based transition. By contrast, the Cl-Ru-O-C torsion angle is equal to 30 degrees in **5a**, arising from hindrance effect induced by the ethyl chain. Theferore, the *p* orbital of the oxygen atom (117, HOMO) can overlap with orbital 120 (LUMO+2, RuNO

fragment), thus adding a significant contribution to the charge transfer towards the nitrosyl.

Table 6 Main electron transitions, with absorption maxima (λ_{max}) oscillator strength (f) and composition of the configuration interaction, computed by TD-DFT for the **3a-b**, **4a**-**b**, and **5a**-**b**.

Compounds	UV-vis spectra	transitions	λ_{max} (nm)	f	main composition[a]	character
cis-**3a**	330 nm	1 → 12	299	0.528	60 % $\chi_{113\rightarrow114}$	phenyl → RuNO
trans-**3a**	350 nm	1 → 10	312	0.363	71 % $\chi_{113\rightarrow114}$	phenyl → RuNO
cis-**3b**	363 nm	1 → 7	335	0.657	49 % $\chi_{114\rightarrow115}$	thiophenyl → RuNO
trans-**3b**	387 nm	1 → 8	348	0.607	74 % $\chi_{114\rightarrow115}$	thiophenyl → RuNO
	361 nm	1 → 9	327	0.138	39 % $\chi_{113\rightarrow115}$ + 26 % $\chi_{111\rightarrow115}$	R-tpyRuCl_2 → RuNO
4a	325 nm	1 → 10	292	0.469	61 % $\chi_{109\rightarrow110}$	phenyl → RuNO
4b	358 nm	1 → 8	327	0.751	68 % $\chi_{110\rightarrow111}$	thiophenyl → RuNO
5a	328 nm	1 → 12	291	0.194	50 % $\chi_{117\rightarrow120}$ + 21 % $\chi_{116\rightarrow118}$	EtO → RuNO
		1 → 13	289	0.250	31 % $\chi_{117\rightarrow120}$ + 24 % $\chi_{116\rightarrow118}$	EtO + phenyl → RuNO
5b	362 nm	1 → 9	327	0.706	39 % $\chi_{118\rightarrow119}$ + 33 % $\chi_{117\rightarrow119}$	EtO + thiophenyl → RuNO

[a] Orbital 113(114) is the HOMO(LUMO) for **3a**, 114(115) the HOMO(LUMO) for **3b**, 109(110) the HOMO(LUMO) for **4a**, 110(111) the HOMO(LUMO) for **4b**, 117(118) the HOMO(LUMO) for **5a**, and 118(119), the HOMO(LUMO) for **5b**.

Figure 6 Selected orbitals and related energies, in the ruthenium nitrosyl complexes **3a**-**b**, **4a**-**b**, and **5a**-**b**. Occupied level are the HOMO orbitals except for **5a**, where orbital 116 is the HOMO-1. Empty levels are the LUMO in any cases.

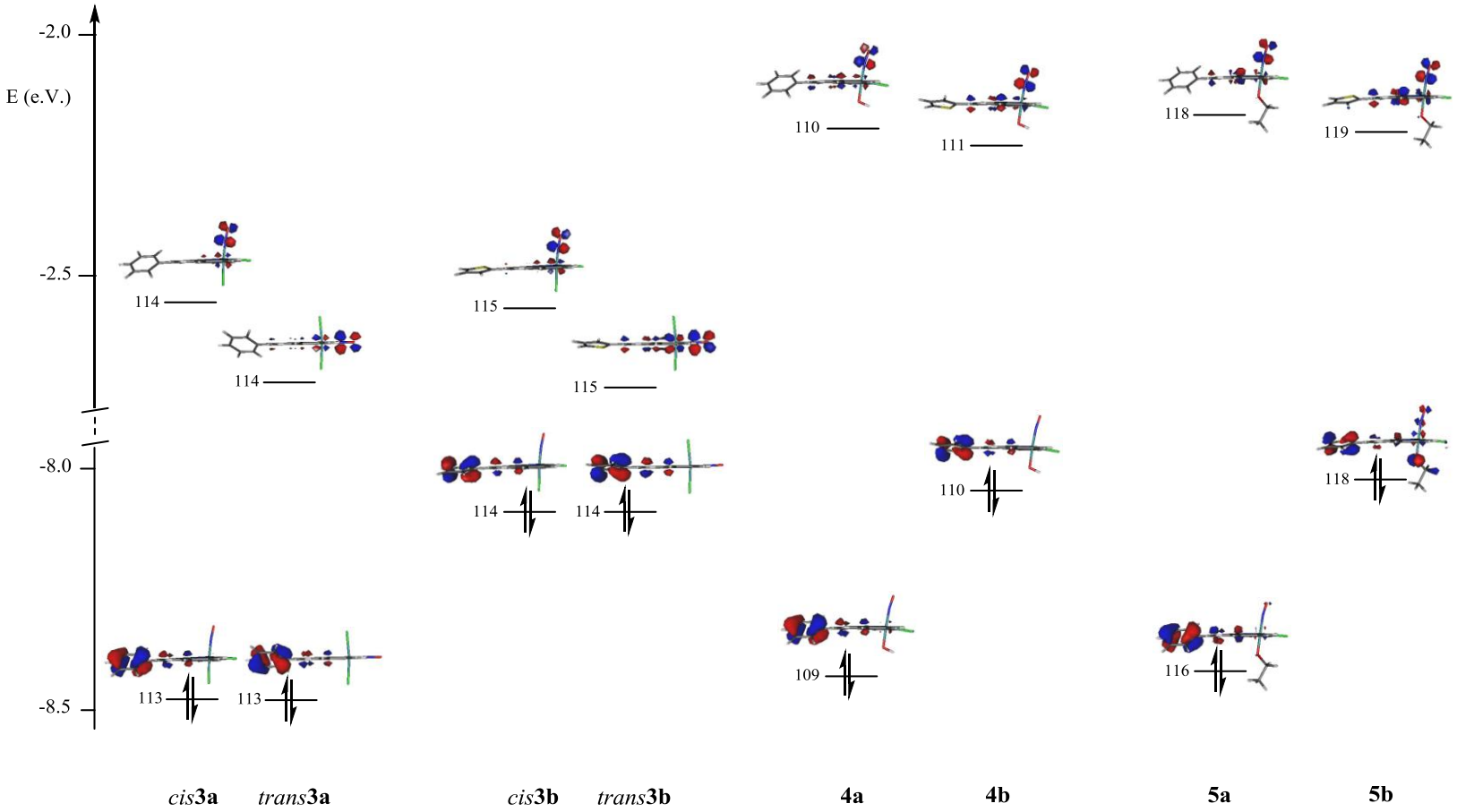

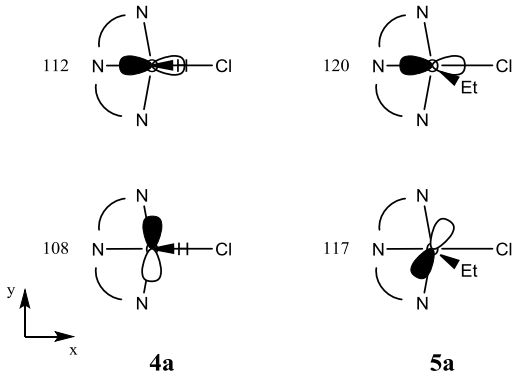

Figure 7. Difference in overlaps between the *p* orbitals of the oxygen atom (bottom) and the d_{xz} orbitals of the ruthenium atom (top), in **4a** (left) and **5a** (right). Orbitals 108(112) are the HOMO-1(LUMO+2) in **4a**, orbitals 117(120) are the HOMO-1(LUMO+2) in **5a**.

NO photo-release

As our investigations have recently started to move towards biological applications,[26] we were interested in studying the photo-release capabilities of this family of complexes in water. However, *cis*-**3a-c** and *trans*-**3a-c** are not stable in water and undergo an evolution towards **4a-c**. For this reason, the photochemical quantum yield (ΦNO) measurements were conducted in both acetonitrile and water, under irradiation at λ = 365 nm. Representative examples for the resulting spectral evolution are shown in Figure 8 with that of **4b** and **5b** featuring the disappearance of the band around λ = 360 nm and the appearance of a new band near λ = 480 nm (details for the experiments on the other complexes can be found in the ESI, Figures S25-28).

The photoreactivity of ruthenium (II) nitrosyl complexes has been well document over the last 40 years and was reviewed by Mascharak.[2] The resulting release of nitric oxide is followed by the formation of a ruthenium (III) photoproduct according to the following equation:

$$[(L)Ru^{II}\text{-}NO+] + \text{solvent} \xrightarrow{h\nu} [(L)Ru^{III}\text{-solvent}] + NO^{\cdot} \qquad (5)$$

Owing to the presence of apparent isosbestic points, which suggest the formation of a single product up to 10 minutes of irradiation, and taking into account our previous observation of the efficient substitution of NO· by MeCN after irradiation of **3c** in acetonitrile,[16b] it can be assumed that the photoproducts obtained in water correspond to the formula $[R\text{-tpyRuIII(Cl)(OH)}(H_2O)]^+$, with the introduction of a molecule of water in the coordination sphere of the ruthenium center. No other investigations were conducted to clarify non-ambiguously on the nature and exact structure of the photoproduct obtained in water. However, various techniques provide evidences that the observed photoreaction corresponds to the NO· release depicted in equation (5). There are hereafter illustrated in the series of *trans*-**3b**, **4b** and **5b** thiophenyl containing compounds as representative examples of the $[Ru(R\text{-tpy})Cl_2NO]^+$, $trans(NO,OH)\text{-}[Ru(R\text{-tpy})(NO)(OH)Cl]^+$ and $trans(NO,OEt)\text{-}[Ru(R\text{-tpy})(NO)(OEt)Cl]^+$ families, respectively. These representative experiments are gathered in Figure 9 (details for the experiments on the other complexes can be found in the ESI, Figure S30). In the case of *trans*-**3b**, the NO· release is evidenced by the use of the Griess test which consists of the observation of an azo dye with strong absorption at λ = 548 nm, generated by the reaction of NO_2^- (oxidized form of NO·) through in situ reaction with sulfanilic acid (Figure 9a).[37]

Alternatively, the NO· release from **4b** can be detected directly and quantitatively in water by the use of a NO· sensor (Figure 9b), in which the resulting chronoamperogram indicates NO· concentration up to 125 nM. Finally, in the case of **5b**, EPR spectroscopy allowed a direct observation of NO· grafted on a spin trap complex $[Fe^{II}(MGD)_2]$ after photorelease induced by irradiation with a Hg lamp. The resulting triplet signal possesses a *g*-factor of 2.040, and a hyperfine coupling constant of $a_N = 1.2 \times 10^{-3}$ cm^{-1}, which are in good agreement with the values reported in the literature (Figure 9c).[38]

The quantum yields of photo-release (ϕ_{NO}), which correspond to the to the number of NO· released per [Ru(NO)]* excited states promoted under irradiation, are gathered in Table 7. In the case of **3a**-**b**, which are not stable in water for a long period of time, no ϕ_{NO} values can be measured precisely.

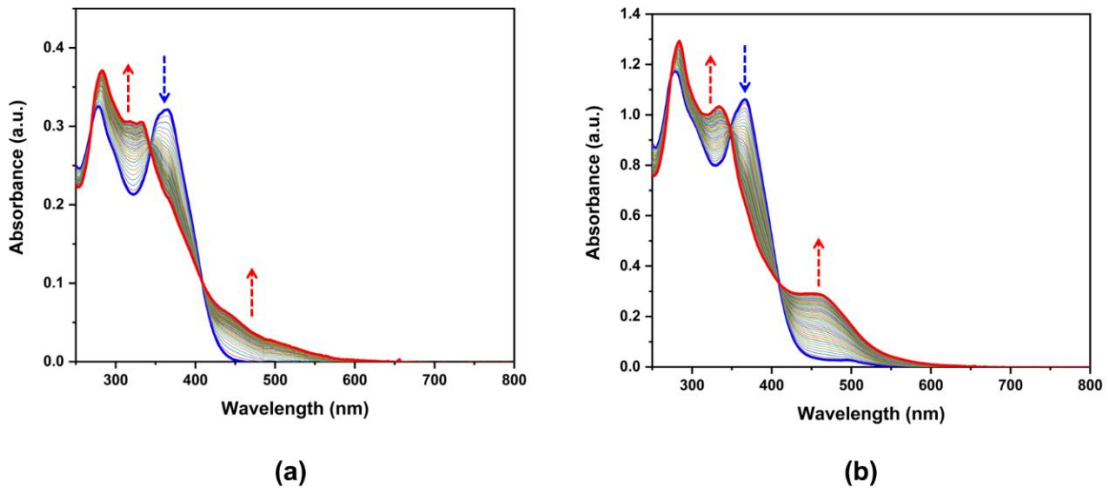

Figure 8 Evolution of the absorption of spectra of (a) **4b** and (b) **5b** in water (0.5 % DMSO) under irradiation at room temperature (λ = 365 nm, 10 min).

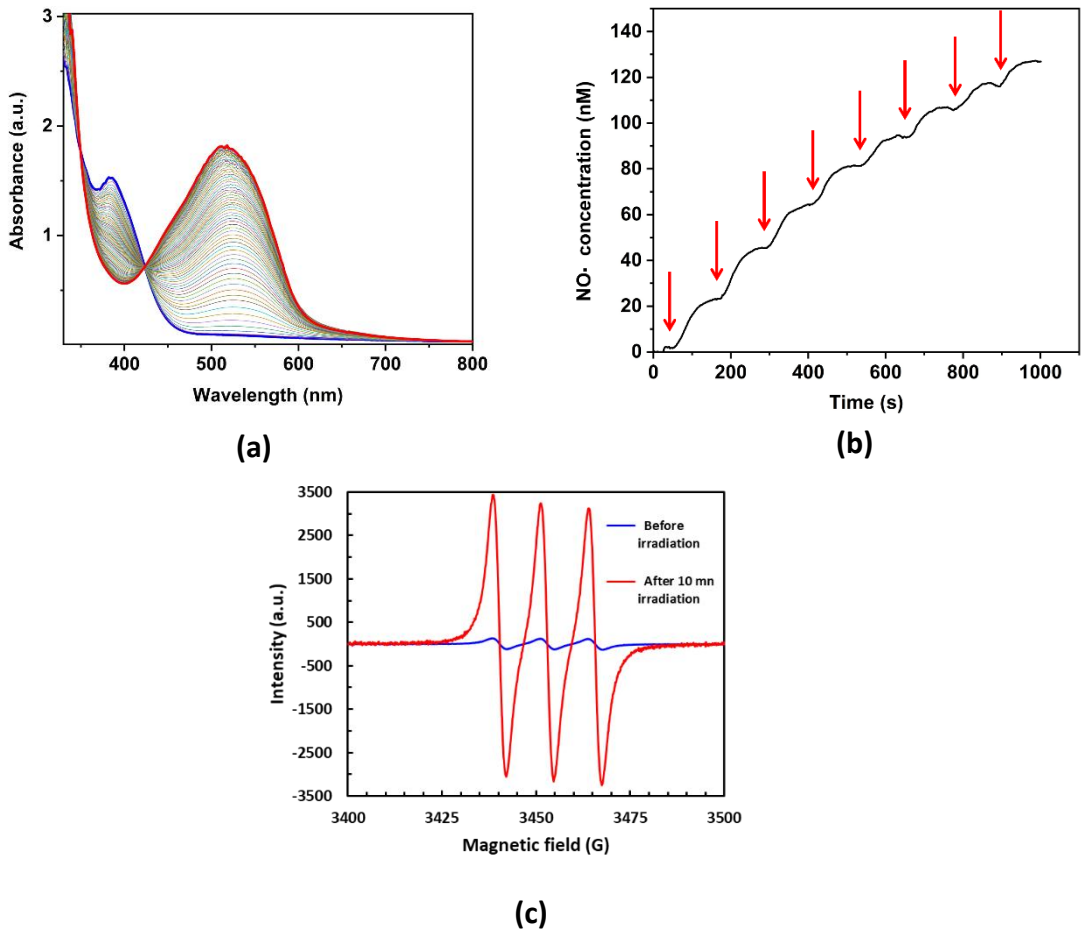

Figure 9 Representative experiments evidencing NO· photo-release (a) Evolution of the electronic spectra for *cis*-**3a** in acetonitrile showing the formation of the azo dye after irradiation at λ = 365 nm in the presence of the Griess Reagent. (b) Chronoamperograms of NO· release upon irradiation of **4b** (400 nM in water) at λ = 365 nm during steps of 15 s (red arrows) every 110 s. (c) Triplet EPR signal after irradiation of **5b** (in acetonitrile) with a Hg lamp (λ > 400 nm) in the presence of the NO·selective $[Fe^{II}(MGD)_2]$ spin trap.

Table 7 Quantum yield of photorelease (ϕ_{NO}) under irradiation at λ = 365 nm.

	3a		**3b**		**4a**	**4b**	**4c**	**5a**	**5b**
	cis	*trans*	cis	*trans*					
ϕ_{NO} in MeCN	0.37[a]	0.12[a]	0.37	0.18	0.18	0.17	0.15	0.38	0.15
ϕ_{NO} in H_2O	-	-	-	-	0.17	0.075	0.04	0.09	0.10

[a] Ref. 17

As can be seen, although a direct correlation of Φ_{NO} with structural features are not evident, all these complexes displays satisfactory NO· photo-release efficiencies, with ϕ_{NO} values higher than 0.12 in acetonitrile, in any case. There is a clear tendency for reduced ϕ_{NO} values in water, although the magnitude of the lowering change significantly from one compound to another.

EXPERIMENTAL SECTION

Materials and equipment

All starting materials were obtained from Alfa-Aesar; the solvents were of analytical grade and used without further purification. Compounds **1a**-**c**,[16a,28,39] **2a**-**c**,[16a,17,40] **3a**,[17] and **3c**[16a] were obtained following modified literature protocols; spectroscopic data were in good agreement. NMR spectra were recorded a Bruker Avance 400 spectrometer at 298 K using deuterated solvents; chemical shifts for ^{1}H- and ^{13}C-NMR data are relative to the residual nondeuterated solvent signal, fixed at δ = 7.26 ppm ($CDCl_3$), δ = 1.940 (CD_3CN) for ^{1}H-NMR and δ = 77.00 ppm ($CDCl_3$), δ = 1.320 (CD_3CN) for ^{13}C-NMR. Coupling constants (J) values are given in Hertz. Infrared spectra were recorded on a Perkin Elmer Spectrum 100 FT-IR spectrometer, using a diamond ATR. The UV-visible spectra were obtained on a Hewlett Packard 8454A spectrometer. HRMS data was acquired using an Agilent G1969A MS TOF spectrometer Elemental analyses were performed at LCC using a Perkin Elmer 2400 series II Instrument.

Syntheses

4'-Phenyl-2,2':6',2''-terpyridine (**1a**). To a stirring solution of benzaldehyde (2 g, 18.8 mmol) in ethanol (65 mL) was added a solution of 2-acetylpyridine (4.2 mL, 37.6 mmol) and KOH (2.110 g, 37.6 mmol) in ethanol (60 mL) previously stirred at room temperature for 30 minutes. The resulting mixture was allowed to stir 15 minutes, followed by addition of 25 % NH_4OH (40 mL) and heating to reflux for 7 hours. The reaction was chilled using an ice/water bath and the resulting precipitate was collected, washed with water and cold ethanol. After recrystallization from boiling ethanol, 3.742 g (64 %) of **1a** as a white solid were obtained. **^{1}H-NMR** δ (400 MHz, $CDCl_3$): 8.75 (s, 2H, H-7), 8.73 (ddd, *J* = 4.8, 1.7, 0.8 Hz, 2H, H-1), 8.67 (d, *J* = 8.0 Hz, 2H, H-4), 7.93-7.90 (m, 2H, H-2'), 7.87 (td, *J* = 7.7, 1.8 Hz, 2H, H-3), 7.51 (t, *J* = 7.3 Hz, 2H, H-3'), 7.45 (t, *J* = 7.3 Hz, 1H, H-4') 7.34 (ddd, *J* = 7.5, 4.8, 1.1 Hz, 2H, H-2). **HRMS** (ESI-TOF$^+$) Anal. calcd. for $C_{21}H_{16}N_3$: 310.1339. Found: 310.1340. Error: 0.5 ppm.

4'-(Thien-2-yl)-2,2':6',2''-terpyridine (**1b**). Synthesized as described above for **1a**, from 2-thiophenecarboxaldehyde. The ligand was obtained in 52 % yield as a pale green solid**.** **^{1}H-NMR** δ (400 MHz, $CDCl_3$): 8.74 (ddd, *J* = 4.8, 1.6, 0.8 Hz, 2H, H-1), 8.69 (s, 2H, H-7), 8.64 (dt, *J* = 7.8, 0.9 Hz, 2H, H-4) , 7.86 (td, *J* = 7.7, 1.8 Hz, 2H, H-3), 7.77 (dd, *J* = 3.7, 1.1 Hz, 1H, H-3') , 77.44 (dd, *J* = 5.0, 1.0 Hz, 1H, H-5'), 7.35 (ddd, *J* = 7.5, 4.8, 1.1 Hz, 2H, H-2), 7.17 (dd, *J* = 5.0, 3.7 Hz, 1H, H-4'). **HRMS** (ESI-TOF$^+$) Anal. calcd. for $C_{19}H_{14}N_3S$: 316.0903. Found: 316.0904. Error: 0.5 ppm.

4'-(9H-fluoren-2-yl)-2,2':6',2''-terpyridine (**1c**). To a suspension of *9H*-fluorene-2-carbaldehyde (1.50 g, 7.72 mmol) and 2-acetylpyridine (0.86 mL, 7.72 mmol) in methanol (11.6 mL), aqueous NaOH (1 M, 7.7 mL) was added dropwise at 0 °C under magnetic. After stirring 7 hours at room temperature, the yellow precipitate formed was collected, washed with water and cold methanol to yield 1.26 g (4.24 mmol) of (E)-3-(*9H*-fluoren-2-yl)-1-(pyridin-2-yl)prop-2-en-1-one as a yellow solid.[41] An ethanolic (20 mL) solution of this intermediate was refluxed in the presence of 1-[2-oxo-2-(2-pyridinyl)ethyl]pyridinium iodide[42] (1.38 g, 4.24 mmol) and NH_4OAc (4.25 g, 55 mmol) overnight to yield a greenish solid, which was purified by column chromatography (hexanes/ethyl acetate 7/3) to yield 1.40 g (3.52 mmol, 46 %) of the title compound as a yellow solid. **^{1}H-NMR** δ (400 MHz, $CDCl_3$): δ 8.80 (s, 2H, H-7), 8.75 (ddd, *J* = 4.8, 1.7, 0.8 Hz, 2H, H-1), 8.69 (dt, *J* = 8.0, 1.0 Hz, 2H, H-4), 8.10 (d, *J* = 0.8 Hz, 1H, H-1'), 7.95 (dd, *J* = 8.0, 1.6 Hz, 1H, H-3'), 7.90-7.86 (m, 3H, H-3, H-4'), 7.84 (d, *J* = 7.5 Hz, 1H, H-5'), 7.58 (d, *J* = 7.4 Hz, 1H, H-8'), 7.41 (t, J = 7.1 Hz, 1H, H-6'), 7.37-7.32 (m, 3H, H-2, H-7'), 3.99 (s, 2H, H-9'). **HRMS** (ESI-TOF$^+$) Anal. calcd. for $C_{28}H_{20}N_3$: 398.1652. Found: 398.1656. Error: 1.1 ppm.

*[Ru^{III}(**1a**)Cl_3]* (**2a**). A mixture of **1a** (812 mg, 2.62 mmol), $RuCl_3 \cdot xH_2O$ (0.523 g) and ethanol (70 mL) was stirred under reflux for 6.5 hours. Then, the mixture was concentrated *in*

vacuo and chilled to 0 °C in a freezer. The resulting red precipitate was collected, washed with chilled ethanol and diethyl ether. The wine-colored crude product was subsequently washed twice with boiling ethanol (50 mL) to yield 852 mg (1.65 mmol, 63 %) of **2a** as a black solid. **Elemental Analysis** found: C, 48.07; H, 2.73; N, 7.77. Required for $C_{21}H_{15}Cl_3N_3Ru$, $1/2H_2O$: C, 47.97; H, 3.07; N, 7.99.

*[Ru^{III}(**1b**)Cl$_3$]* (**2b**). Synthesized as describe above for **2a**, from ligand **1b**. The title complex was obtained in 76 % yield as a black solid. **Elemental Analysis** found: C, 42.72; H, 2.22, N, 7.71. Required for $C_{19}H_{13}Cl_3N_3RuS$, $1/2H_2O$: C, 42.91; H, 2.65; N, 7.90.

*[Ru^{III}(**1c**)Cl$_3$]* (**2c**). Synthesized as describe above for **2a**, from ligand **1c**. The title complex was obtained in 95 % yield as a black solid. **Elemental Analysis** found: C, 51.53; H, 2.98; N, 6.33. Required for $C_{28}H_{19}Cl_3N_3Ru$, $2.5H_2O$: C, 51.74; H, 3.72; N, 6.47.

*Preparation of the mixture of isomers cis(Cl,Cl)- and trans(Cl,Cl)-[Ru^{II}(**1a**)(NO)Cl$_2$](Cl) complexes* (**3a**). Compound **2a** (822 mg, 1.59 mmol) was dissolved in dimethylformamide (125 mL) and warmed up to 85 °C. Gaseous nitric oxide, obtained by the dropwise addition of diluted HNO_3 on copper, was bubbled under argon atmosphere during 3-5 hours. The reaction mixture was allowed to cool down to room temperature and it was concentrated *in vacuo* to a final volume of *ca.* 10 mL. After addition of a large excess of diethyl ether, 802 mg of a pale orange powder were obtained (1.47 mmol, 92 %). As evidenced by ^{1}H-NMR , this crude product was mainly (> 98 %) constituted by a mixture of two species, namely the *cis(Cl,Cl)-[Ru^{II}(**1a**)(NO)Cl$_2$](Cl)* (*cis*-**3a**) and *trans(Cl,Cl)-[Ru^{II}(**1a**)(NO)Cl$_2$](Cl)* (*trans*-**3a**) isomers in a *trans*/*cis* 7/3 ratio (See SI Figure S1). This mixture was consequently used for the following reactions without any further purification.

*Preparation of the mixture of isomers cis(Cl,Cl)- and trans(Cl,Cl)-[Ru^{II}(**1b**)(NO)Cl$_2$](Cl) complexes* (**3b**). Prepared as described above for **3a** from complex **2b**. The yield of the crude orange-ish product was 97 %. According to ^{1}H-NMR , this crude mixture was mainly (> 98 %) constituted by the *cis(Cl,Cl)-[Ru^{II}(**1b**)(NO)Cl$_2$](Cl)* (*cis*-**3b**) and *trans(Cl,Cl)-[Ru^{II}(**1b**)(NO)Cl$_2$](Cl)* (*trans*-**3b**) isomers in a *trans*/*cis* 7/3 ratio (See SI Figure S2). Analytical samples of both *cis*-**3b** and *trans*-**3b** isomers were isolated as their PF_6 salts after HPLC purification followed by metathesis employing aqueous NH_4PF_6.

*cis(Cl,Cl)-[Ru^{II}(**1b**)(NO)Cl$_2$](PF$_6$)* (*cis*-**3b**). Pale yellow solid **^{1}H-NMR** δ (400 MHz, CD_3CN): 9.18 (ddd, *J* = 5.5, 1.5, 0.5 Hz, 2H, H-1), 8.73 (ddd, *J* = 8.1, 1.2, 0.6 Hz, 2H, H-4), 8.69 (s, 2H, H-7), 8.48 (td, *J* = 7.9, 1.6 Hz, 2H, H-3), 8.17 (dd, *J* = 3.8, 1.1 Hz, 1H, H-3'), 7.99 – 7.91 (m, 3H, H-2, H-5'), 7.40 (dd, *J* = 5.0, 3.8 Hz, 1H, H-4'). **^{13}C-NMR** δ (100 MHz, CD_3CN): 158.38 (C-5), 154.79 (C-6), 154.22 (C-1), 150.07 (C-8), 143.75 (C-3), 139.18 (C-2'), 134.25 (C-5'), 132.14 (C-3'), 130.95 (C-4'), 130.51 (C-2), 127.48 (C-4), 121.66 (C-7). **FT-IR** (ATR, cm^{-1}): 1887 (νNO). **Elemental Analysis** found: C, 34.47; H, 1.33; N, 8.70. Required for $C_{19}H_{13}Cl_2N_4ORuS$, PF_6: C, 34.46; H, 1.98; N, 8.46. **HRMS** (ESI-TOF$^+$) Anal. calcd. for $C_{19}H_{13}Cl_2N_4ORuS$: 516.9231. Found: 516.9232. Error: 0.2 ppm. **UV-vis** λ_{max} in nm (ε in M^{-1}cm^{-1}): 281 (21568), 363 (18682).

*trans(Cl,Cl)-[Ru^{II}(**1b**)(NO)Cl$_2$](PF$_6$)* (*trans*-**3b**). Yellow solid. **^{1}H-NMR** δ (400 MHz, CD_3CN): 8.78 – 8.74 (m, 2H, H-1), 8.67 (d, *J* = 8.1 Hz, 2H, H-4), 8.60 (s, 2H, H-7), 8.38 (td, *J* = 7.8, 1.3 Hz, 2H, H-3), 8.16 (dd, *J* = 3.8, 1.0 Hz, 1H, H-3'), 7.95 (dd, *J* = 4.7, 0.9 Hz, 1H, H-5'), 7.87 (ddd, *J* = 7.5, 5.4, 1.2 Hz, 2H, H-2), 7.39 (dd, *J* = 4.7, 3.8 Hz, 1H, H-4').**^{13}C-NMR** δ (100 MHz, CD_3CN): 154.90 (C-5), 154.10 (C-1), 153.14 (C-6), 152.95 (C-8), 142.44 (C-3), 138.05 (C-2'), 133.86 (C-5'), 131.62 (C-3'), 130.08 (C-2), 130.01 (C-4'), 126.70 (C-4), 120.41 (C-7). **FT-IR** (ATR, cm^{-1}): 1913 (νNO). **Elemental Analysis** found: C, 34.49; H, 1.52; N, 8.69. Required for $C_{19}H_{13}Cl_2N_4ORuS$, PF_6: C, 34.46; H, 1.98; N, 8.46. **HRMS** (ESI-TOF$^+$) Anal. calcd. for $C_{19}H_{13}Cl_2N_4ORuS$: 516.9231. Found: 516.9225. Error: -1.2 ppm. **UV-vis** λ_{max} in nm (ε in M^{-1}cm^{-1}): 277 (25201), 361 (17488), 387 (20510).

*Preparation of the mixture of isomers cis(Cl,Cl) and trans(Cl,Cl)-[Ru^{II}(**1c**)(NO)Cl$_2$](Cl) complexes* (**3c**). Prepared as described above for **3a** from complex **2c**. In agreement with previous observations,[17] in this case after stopping the reaction, an orange-ish precipitate was formed which corresponded to the pure *trans*(Cl,Cl) isomer according to ^{1}H-NMR. It was obtained in 28 % yield. The filtrate was concentrated under reduced pressure to yield a second orange powder which corresponded to the mixture of the *cis(Cl,Cl)-[Ru^{II}(**1c**)(NO)Cl$_2$](Cl)* (*cis*-**3c**) and *trans(Cl,Cl)-[Ru^{II}(**1c**)(NO)Cl$_2$](Cl)* (*trans*-**3c**) isomers in a *trans*/*cis* 1/1 ratio (Figure S3). The combined yield was 91 %.

General procedure for the synthesis of trans(NO,OH) complexes in water. In a typical run, 150 mg of the crude *trans*/*cis* mixture of complexes (**3a-c**) were dissolved in boiling water (*ca.* 0.5 mg/mL) followed by reflux overnight. The resulting yellowish solution was concentrated *in vacuo* and treated with a small amount of NH_4PF_6. The cream to yellow solid thus obtained was collected, washed with water and dried. In most cases, at this step ^{1}H-NMR showed complete depletion of the starting material and purity of the desired complex above 95 %. When significant impurities were observed, the product was further purified by preparative TLC on SiO_2 using 1/1 CH_2Cl_2/CH_3CN as an eluent.

*trans(NO,OH)-[Ru^{II}(**1a**)(NO)(OH)Cl](PF$_6$)* (**4a**). Obtained as a yellow solid in 89 % yield. **^{1}H-NMR** δ (400 MHz, CD_3CN): 9.11 (d, *J* = 5.5 Hz, 2H, H-1), 8.74 (s, 2H, H-7), 8.60 (d, *J* = 8.1 Hz, 2H, H-4), 8.39 (t, *J* = 7.9 Hz, 2H, H-3), 8.07 – 8.03 (m, 2H, H-2'), 7.93 – 7.87 (m, 2H, H-2), 7.66 (d, *J* = 4.7 Hz, 3H, H-3',

H-4'), 4.35 (br s, 1H, OH). **^{13}C-NMR** δ (100 MHz, CD_3CN): 158.31 (C-5), 156.62 (C-8), 155.04 (C-6), 153.58 (C-1), 143.38 (C-3), 136.15 (C-1'), 132.75 (C-4'), 130.70 (C-3'), 130.03 (C-2), 129.13 (C-2'), 127.03 (C-4), 123.59 (C-7). **FT-IR** (ATR, cm^{-1}): 1834 (νNO). **Elemental Analysis** found: C, 39.86; H, 2.18; N, 9.90. Required for $C_{21}H_{16}ClN_4O_2RuPF_6$; 1/2 CH_3CN: C, 40.13; H, 2.68; N, 9.57. **HRMS** (ESI-TOF$^+$) Anal. calcd. for $C_{21}H_{16}ClN_4O_2Ru$: 493.0005. Found: 493.0018. Error: 2.6 ppm. **UV-vis** λ_{max} in nm (ε in $M^{-1}cm^{-1}$): 297 (27734), 325 (19660).

*trans(NO,OH)-[Ru^{II}(**1b**)(NO)(OH)Cl](PF$_6$)* (**4b**). Obtained as a yellow solid in 86 % yield. **^{1}H-NMR** δ (400 MHz, CD_3CN): 9.09 (dd, *J* = 5.4, 1.1 Hz, 2H, H-1), 8.57 (s, 2H, H-7), 8.47 (d, *J* = 7.9 Hz, 2H, H-4), 8.30 (td, *J* = 7.9, 1.5 Hz, 2H, H-3), 8.04 (dd, *J* = 3.8, 1.1 Hz, 1H, H-3'), 7.88 (ddd, *J* = 7.6, 5.5, 1.3 Hz, 2H, H-2), 7.81 (dd, *J* = 5.0, 1.0 Hz, 1H, H-5'), 7.21 (dd, *J* = 5.0, 3.8 Hz, 1H, H-4'), 4.46 (br s, 1H, OH). **^{13}C-NMR** δ (100 MHz, CD_3CN): 158.01 (C-5), 154.95 (C-6), 153.48 (C-1), 149.26 (C-8), 143.24 (C-3), 139.12 (C-2'), 133.99 (C-5'), 131.97 (C-3'), 130.83 (C-4'), 130.00 (C-2), 126.91 (C-4), 120.96 (C-7). **FT-IR** (ATR, cm^{-1}): 1857 (νNO). **Elemental Analysis** found: C, 34.98; H, 2.21; N, 8.28. Required for $C_{19}H_{14}ClN_4O_2RuS$, PF_6: C, 35.44; H, 2.19; N, 8.70. **HRMS** (ESI-TOF$^+$) Anal. calcd. for $C_{19}H_{14}ClN_4O_2RuS$: 498.9569. Found: 498.9572. Error: 0.6 ppm. **UV-vis** λ_{max} in nm (ε in $M^{-1}cm^{-1}$): 280 (27000), 358 (21103).

*trans(NO,OH)-[Ru^{II}(**1c**)(NO)(OH)Cl](PF$_6$)* (**4c**). Obtained as a yellow solid in 73 % yield. **^{1}H-NMR** δ (400 MHz, CD_3CN): 9.23 (dd, *J* = 5.7 Hz, 1.4 Hz, 2H, H-1), 8.96 (2H, s, H-7), 8.85 (d, *J* = 8.2 Hz, 2H, H-4), 8.52 (td, *J* = 7.8 Hz, 1.5 Hz, 2H, H-3), 8.40 (s, 1H, H-1'), 8.24 - 8.16 (m, 2H, H-3', H-4'), 8.06 - 7.98 (m, 3H, H-2, H-5'), 7.95 (br s, 1H, OH), 7.72 (d, *J* = 6.8 Hz, 1H, H-8'), 7.55-7.45 (m, 2H, H-6', H-7'), 4.16 (s, 2H, H-9').

General procedure for the synthesis of trans(NO,OEt) complexes. 100 mg of crude samples of complexes **4a-c** were dissolved in 150 mL of absolute ethanol and stirred at 80 °C for 3 hours. The solution was then concentrated to *ca*. 5 mL followed by addition of diethyl ether. The precipitate thus obtained was collected, washed with diethyl ether and dried.

*trans(NO,OEt)-[Ru^{II}(**1a**)(NO)(OEt)Cl](PF$_6$)* (**5a**). Obtained as a pale orange solid in 93 % yield. **^{1}H-NMR** δ (400 MHz, CD_3CN): 9.16 – 9.11 (m, 2H, H-1), 8.76 (s, 2H, H-7), 8.69 (d, *J* = 7.6 Hz, 2H, H-4), 8.45 (td, *J* = 7.9, 1.6 Hz, 2H, H-3), 8.09 – 8.05 (m, 1H, 2H, H-2'), 7.93 (ddd, *J* = 7.7, 5.5, 1.3 Hz, 2H, H-2), 7.73 – 7.68 (m, 3H, H-3', H-4'), 3.84 (q, *J* = 6.9 Hz, 2H, H-9), 0.53 (t, *J* = 6.9 Hz, 3H, H-10). **^{13}C-NMR** δ (100 MHz, CD_3CN): 158.50 (C-5), 156.71 (C-8), 155.00 (C-6), 153.57 (C-1), 143.44 (C-3), 136.47 (C-1'), 132.64 (C-4'), 130.71 (C-3'), 130.14 (C-2), 129.18 (C-2'), 126.99 (C-4), 123.80 (C-7), 66.37 (C-9), 19.80 (C-10). **FT-IR** (ATR, cm^{-1}): 1814 (νNO). **Elemental Analysis** found: C, 41.23; H, 2.75; N, 8.62. Required for $C_{23}H_{20}ClN_4O_2Ru,PF_6$: C, 41.48; H, 3.03; N, 8.41. **HRMS** (ESI-TOF$^+$). Anal. calcd. for $C_{23}H_{20}ClN_4O_2Ru$: 521.03210. Found: 521.0338. Error: 3.26 ppm. **UV-vis** λ_{max} in nm (ε in $M^{-1}cm^{-1}$): 297 (28077), 328 (19315).

*trans(NO,OEt)-[Ru^{II}(**1b**)(NO)(OEt)Cl](PF$_6$)* (**5b**). Obtained as a pale orange solid in 95 % yield. **^{1}H-NMR** δ (400 MHz, CD_3CN): 9.16 – 9.11 (m, 2H, H-1), 8.68 (d, *J* = 8.1 Hz, 2H, H-4), 8.65 (s, 2H, H-7), 8.45 (td, *J* = 7.9, 1.5 Hz, 2H, H-3), 8.15 (dd, *J* = 3.8, 1.1 Hz, 1H, H-3'), 7.95 – 7.90 (m, 3H, H-2, H-5'), 7.39 (dd, *J* = 5.0, 3.8 Hz, 1H, H-4'), 3.82 (q, *J* = 6.9 Hz, 2H, H-9), 0.51 (t, *J* = 6.9 Hz, 3H, H-10). **^{13}C-NMR** δ (100 MHz, CD_3CN): 158.35 (C-5), 155.05 (C-6), 153.56 (C-1), 149.49 (C-8), 143.38 (C-3), 140.48 (C-2'), 133.81 (C-5'), 131.76 (C-3'), 130.84 (C-4'), 130.16 (C-2), 126.97 (C-4), 121.31 (C-7), 66.34 (C-9), 19.78 (C-10). **FT-IR** (ATR, cm^{-1}): 1835 (νNO). **Elemental Analysis** found: C, 37.33; H, 2.24; N, 8.80. Required for $C_{21}H_{18}N_4O_2SRuCl$, PF_6: C, 37.54; H, 2.70; N, 8.34. **HRMS** (ESI-TOF$^+$) Anal. calcd. for $C_{21}H_{18}N_4O_2SRuCl$: 526.9882. Found: 526.9887. Error: 0.9 ppm. **UV-vis** λ_{max} in nm (ε in $M^{-1}cm^{-1}$): 279 (22932), 362 (20347).

Single X-Ray Diffraction studies

Data were collected on a Bruker Kappa Apex II diffractometer equipped with a sealed X-Ray tube source (*cis*-3b and 5b) or with a 30 W air-cooled microfocus source (*trans*-3b, 4a, 4b and 5a), using MoK_α radiation (λ = 0.71073 Å). An Oxford Cryosystems Cryostream cooler device was used to collect the data at low temperature. Phi- and omega- scans were performed for data collection. An empirical absorption correction with SADABS was applied.[43] The structures were solved by intrinsic phasing method (SHELXT),[44] or with SUPERFLIP,[45] and refined by means of least-squares procedures on F² with SHELXL,[46] and on F with CRYSTALS.[47] All non-hydrogen were refined anisotropically. Hydrogen atoms were located in a difference map but those attached to carbon atoms were repositioned geometrically and then refined using a riding model.

CCDC 1968710-1968715 contains the supplementary crystallographic data for this paper. These data can be obtained free of charge from the Cambridge Crystallographic data center.

Computational methods

The molecular geometries of the ruthenium nitrosyl complexes were fully optimized using the Gaussian-09 program package,[48] within the framework of the Density Functional Theory (DFT) at the B3PW91/6-31G* level (See SI, Table S31). B3PW91 was selected following the previous report on ruthenium-nitrosyl by Mascharak,[49] who states that this hybrid functional outperforms other methods in numerous cases of ruthenium complexes, especially when back bonding ligands (like NO) are present.[50] The LANL2DZ pseudo-potential was used to account for relativistic effects on the ruthenium atom.[51] Vibrational analyses were

performed at the same level to verify that the stationary points correspond to minima on the potential energy surfaces. Solvent effects (water, acetonitrile) were modeled by the Polarizable Continuum Model (SCRF=PCM method).[52] The TD-DFT computations of the UV-vis spectra were carried out on the optimized geometries at the CAM-B3LYP/6-31G* level. The CAM-B3LYP and PBE0 methods were tested for consistencies with our previous investigations on Ru(NO) complexes. We observed a tendency for over-estimated transition energies with CAM-B3LYP and under-estimated energies with PBE0. Finally, we selected CAM-B3LYP for which a blue shift is observed for the computed values with average values of 2700 cm^{-1} for the thiophenyl containing species and 3500 cm^{-1}, for the phenyl containing complexes. Although significantly larger than the commonly found discrepancy of 2500 cm^{-1} observed in small organic molecules, the present values are still acceptable due to large molecular sizes, heavy ruthenium atoms, and sizeable charge transfer effects.[53] Molecular orbitals were plotted by using the GABEDIT free software.[54,55]

NO calibration

The quantitative determination of NO production was performed with a commercial NO detector (ami-NO 700) from Innovative Instruments Inc. Calibration of the electrode in the range of 50–1000 nM was performed by generating NO according to the following reaction:

$$2NO_2^- + 4H^+ + 2I^- \rightarrow 2NO^{\cdot} + I_2 + 2H_2O \qquad (6)$$

For each calibration, aliquots (80 µL) of aqueous $NaNO_2$ (~100 µM) were added to 20 mL of a 0.03 $mol.L^{-1}$ solution of KI in 0.1 $mol.L^{-1}$ H_2SO_4. Chronoamperograms were registered at a fixed temperature (25 °C) while stirring the solution in order to maintain a constant rate of oxidation of the produced NO at the electrode surface. The typical sensitivity of the electrode was about 100 pA/nM. During the photolysis measurements, the NO sensor was positioned outside the light path. Besides, chronoamperograms of an aqueous solution were systematically registered upon irradiation in order to substract the light interference. Then, chronoamperograms were registered upon irradiation of 20 mL of an aqueous solution of each complex in steps of 15 s every 110 s in order to stabilize the intensity between each step.

Photochemistry

Kinetic studies on the photolysis reactions were carried out with a diode array Hewlett Packart 8454A spectrophotometer. The optical fiber was fixed laterally from the cuvette. Absorption spectra were taken after each minute, in fast scan mode. The UV-visible spectra were recorded under irradiation realized with a Muller reactor device equipped with a cooling water filter and monochromatic LEDs (see above). The light intensity was determined by using a power-meter from Thorlabs (PM100D). The sample solutions were placed in a quartz cuvette of 1 cm path -length stirred continuously. The temperature was maintained at 25 °C during the whole experiment.

Quantum yield measurements: The quantum yield (φ_A) was determined by the program Sa3.3 written by D. Lavabre and V. Pimienta.[56,57] It allows the resolution of the differential equation :

$$\frac{d[Ru^{II}]}{dt} = -\Phi \cdot \varepsilon_{Ru^{II}} \cdot [Ru^{II}] \cdot I_0 \cdot l_{irr} \cdot F \qquad (7)$$

Where F is the photokinetic factor $F = (1–10^{-Abs})/Abs$ with $\mathrm{Abs} = (\varepsilon_{Ru^{II}} \cdot [Ru^{II}] + \varepsilon_{Ru^{III}} \cdot [Ru^{III}]) \cdot l_{irr}$, Φ is the photochemical quantum yield, I_0 is the incident photon flux (in mol L^{-1} s^{-1}), $\varepsilon_{Ru^{II}}$ (in mol^{-1} L cm^{-1}) is the molar extinction coefficient of the ruthenium nitrosyl complexes and l_{irr} is the length of the optical irradiation path. The equation was fitted with the experimental data Abs = ƒ(t) and 2 parameters φ_A and ε_B (ε_B is the molar extinction coefficient measured at the end of the reaction). λ_{obs} was chosen to correspond to a large difference between molar extinction coefficient at the initial and final time of the photochemical reaction. Simulation and optimization procedures were performed by using numerical integration and a non-linear minimization algorithm for the fitting of the model to the experimental data. (See SI, Table S32).

CONCLUSION

We have investigated a set of *cis*(Cl,Cl)- and *trans*(Cl,Cl)-ruthenium nitrosyl complexes built up from various substituted terpyridine ligands, initially regarded as optical materials. The full characterization of such systems implies the separation of the *cis*/*trans* isomers at the end of the synthetic process. By contrast, their behavior in water indicates the irreversible substitution of one chloride by one hydroxo ligand leading to a single and stable *trans*(NO,OH) isomer, in any case, thus avoiding the tedious separation step, encountered in L-$RuCl_2$(NO) chemistry. Moreover, the resulting water stable species exhibit $NO^{\cdot}$ release capabilities under irradiation, which indicate potential uses in biological media, in relation to the widely recognized importance of nitric oxide in biology.

CONFLICTS OF INTEREST

The authors state that there are no conflicts to declare.

ACKNOLEDGMENTS

The work has been performed within the framework of the French-Mexican International Laboratory (LIA-LCMMC). The authors thank Carine Duhayon (LCC-CNRS) for her help in the record of X-Ray data, and acknowledge the financial

supports of CNRS (France), CONACyT (Mexico), and PAPIIT (Mexico). PLV thanks CONACyT for an academic scholarship (337958). MB thanks the University Paul Sabatier (COMUE) and the Région Midi-Pyrénées through the RuNOthérapie grant.

NOTES AND REFERENCES

1 (a) Ph. Coppens, I. Novozhilova and A. Kovalevsky, *Chem. Rev.*, 2002, **102**, 861. (b) L. Khadeeva, W. Kaszub, M. Lorenc, I. Malfant and M. Buron-Le Cointe, *Inorg. Chem.*, 2016, **55**, 4117. (c) A.A. Mikhailov, E. Wenger, G.A. Kostin and D. Schaniel, *Chem. Eur. J.*, 2019, **25**, 7569.

2 (a) N.L. Fry and P.K. Mascharak, *Acc. Chem. Res.*, 2011, **44**, 289. (b) M.J. Rose and P.K. Mascharak, *Coord. Chem. Rev.*, 2008, **252**, 2093. (c) M.J. Rose and P.K. Mascharak, *Curr. Opin. Chem. Biol.*, 2008, **12**, 238.

3 (a) E. Tfouni, M. Krieger, B.R. McGarvey and D.W. Franco, *Coord. Chem. Rev.,* 2003, **236**, 57-69. (b) E. Tfouni, D.R. Truzzi, A. Tavares, A.J. Gomes, L.E. Figueiredo and D.W. Franco, *Nitric Oxide*, 2012, **26**, 38.

4 (a) D. Schaniel, B. Cormary, I. Malfant, L. Valade, T. Woike, B. Delley, K. W. Kraemer and H.-U. Guedel, *Phys. Chem. Chem. Phys.,* 2007, **9**, 3717. (b) B. Cormary, I. Malfant, M. Buron-Le Cointe, L. Toupet, B. Delley, D. Schaniel, N. Mockus, T. Woike, K. Fejfarova, V. Petricek and M. Dusek, *Acta Crystallogr. Sect. B,* 2009, **65**, 612. (c) B. Cormary, S. Ladeira, K. Jacob, P.G. Lacroix, T. Woike, D. Schaniel and I. Malfant, *Inorg. Chem.,* 2012, **51**, 7492.

5 P. Günter and J. P. Huignard, Photorefractive materials and their application. ed.; Springer: Berlin, 1988.

6 T. Woike, W. Kirchner, G. Shetter, T. Barthel, K. Hyung-sang and S. Haussühl, *Opt. Commun.,* 1994, **106**, 6.

7 J. Ashley, M.-P. Bernal, G. W. Burr, H. Coufal, H. Guenther, J. A. Hoffnagle, C. M. Jefferson, B. Marcus, R. M. Macfarlane and R. M. Shelby, *IBM J. Res. Develop.,* 2000, **44**, 341.

8 S. Kawata and Y. Kawata, *Chem. Rev.,* 2000, **100**, 1777.

9 L.J. Ignarro, Nitric oxide biology and pathobiology, Academic Press, San Diego, 1st edn, 2000.

10 S. Singh and A.K. Gupta, *Cancer Chemother. Pharmacol.*, 2011, *67*, 1211.

11 Dialing "ruthenium nitrosyl" as a key word in the SciFinder data base leads to a number of annual entries within the general topic of "NO· release", which was roughly multiplied by 5 during the last 20 years.

12 H.J. Xiang, M. Guo, J.G. Liu, *Eur. J. Inorg. Chem*. 2017, 1586-1595.

13 Nitrosyl Complexes in Inorganic Chemistry, Biochemistry and Medicine. Structure and Bonding (special issue), ed. Springer, Berlin Germany, 2014, vol. 153 - 154.

14 P.C. Ford, *Acc. Chem. Res.* 2008, **41**, 190-200

15 for recent reports on NO· release from ruthenium nitrosyl complexes, see: (a) Mikhailov, A.A.; Vorobyev, V.A.; Nadolinny, V.A.; Patrushev, Y.V.; Yudina, Y.S.; Kostin, G.A. J. Photochem. Photobiol A, Chemistry 2019, 373, 37-44. (b) Orlowska, E.; Babak, M.V. Doemoetoer, O.; Enyedy, E.A.; Rapta, P.; Zalibera, M.; Bucinsky, L.; Malcek, M.; Govind, C.; Karunakaran, V.; Shaik Farid, Y.C.; McDonnell, T.E.; Luneau, D.; Schaniel, D.; Han Ang, W.; Arion, V.B. Inorg. Chem. 2018, 57, 10702-10717. (c) Crisalli, M.A.; Franco, L.P.; Silva, B.R.; Holanda, A.K.M.; Bendhack, L.M.; Da Silva, R.S.; Ford, P.C. J. Coord. Chem. 2018, 71, 1690-1703, (d) Kumar, R.; Kumar, S.; Bala, M.; Ratnam, A.; Singh, U.P.; Ghosh, K. J. Organomet. Chem. 2018, 863, 77-83; (e) Guo, M.; Xiang, H.J.; Wang, Y.; Zhang, Q.L.; An, L.; Yang, S.P.; Ma, Y.; Wang, Y.; Liu, J.G. Chem. Commun. 2017, 53, 3253-3256

16 (a) J. Akl, I. Sasaki, P.G. Lacroix, I. Malfant, S. Mallet-Ladeira, P. Vicendo, N. Farfán and R. Santillan, *Dalton Trans.,* 2014, **45**, 12721. (b) J. Akl, I. Sasaki, P.G. Lacroix, V. Hugues, P. Vivendo, M. Bocé, S. Mallet-Ladeira, M. Blanchard-Desce and I. Malfant, *Photochem. Photobiol., Sci.* 2016, **15**, 1484.

17 S. Amabilino, M. Tassé, P.G. Lacroix, S. Mallet-Ladeira, V. Pimienta, J. Akl, I. Sasaki and I. Malfant, *New J. Chem.,* 2017, **41**, 7371.

18 M. Pawlicki, H.A. Collins, R.G. Denning, H.L. Anderson, *Angew. Chem. Int. Ed.*, 2009, **48**, 3244.

19 B. Strehmel and V. Strehmel, "Two-photon physical, organic, and polymer chemistry: theory, techniques, chromophore design, and applications" in *Advances in Photochemistry*, Neckers, D.C.; Jenks W.S.; Wolff, Th. eds., J. Wiley & Sons, Inc. 2007, Vol. 29, pp. 111-341.

20 E.W. Van Stryland and M. Sheik-Bahae, in *Characterization Techniques and Tabulations for Organic Nonlinear Material*s (Eds.: M.G. Kuzyk, C.W. Dirk), Marcel Dekker, Inc., 1998, p. 655-682.

21 (a) A. Enriquez-Cabrera, I. Sasaki, V. Bukhanko, M. Tassé, S. Mallet-Ladeira, P.G. Lacroix, R.M. Barba-Barba, G. Ramos, N. Farfán, Z. Voitenko and I. Malfant, *Eur. J. Inorg. Chem.,* 2017, 1446. (b) A. Enriquez-Cabrera, P.G. Lacroix, I. Sasaki, S. Malet-Ladeira, N. Farfan, R.M. Barba-Barba, G. Ramos-Ortiz and I. Malfant, *Eur. J. Inorg. Chem.,* 2018, 531. (c) M. Roose, I. Sasaki, V. Bukhanko, S. Mallet-Ladeira, R.M. Barba-Barba, G. Ramos-Ortiz, A. Enriquez-Cabrera, N. Farfán, P.G. Lacroix and I. Malfant, *Polyhedron,* 2018, **151**, 100.

22 Ch.B. Marble, J.E. Clary, G.D. Noojin, S.P. O'Connor, D.T. Nodurft, A.W. Wharmby, B.A. Rockwell, M.O. Scully and V.V. Yakovlev, *Opt. Lett.,* 2018, **43**, 4196.

23 A.V. Sokolov, L.M. Naveira, M.P. Poudel, J. Strohaber, C.S. Trendafilova, W.C. Buck, J. Wang, B.D. Strycker, C. Wang, H. Schuessler, A. Kolomenskii and G.W. Kattawar, *Appl. Optics,* 2010, **49**, 513.

24 K. Kamada, K. Matsunaga, A. Yoshino and K. Ohta, *J. Opt. Soc. Am. B,* 2003, **20**, 529.

25 A. Dragonmir, J.G. McInerney and D.N. Nikogosyan, *Appl. Opt.,* 2002, **41**, 4365.

26 M. Bocé, M. Tassé, S. Mallet-Ladeira, F. Pillet, Ch. Da Silva, P. Vicendo, P.G. Lacroix, I. Malfant and M.P. Rols, *Sci. Rep.,* 2019, **9**, 1.
27 W. Zecher and F. Kröhnke, *Chem. Berichte,* 1961, **94**, 690.
28 J. Wang and G. S. Hanan, *Synlett,* 2005, **8**, 1251.
29 D. H. McDaniel and H. C. Brown, *J. Org. Chem.,* 1958, **23**, 420.
30 J. H. Enemark and R. D. Feltham, *Coord. Chem. Rev.,* 1974, **13**, 339.
31 M.O. Sinnokrot and C.D. Sherrill, *J. Phys. Chem. A,* 2004, **108**, 10200.
32 S. E. Wheeler and J.W.G. Bloom, *J. Phys. Chem. A,* 2014, **118**, 6133.
33 J.B. Godwin and T. Meyer, *Inorg. Chem.,* 1971, **10**, 471.
34 K. Karidi, A. Garoufis, N. Hadjiliadis, M. Lutz, L. Spek and J. Reedijk, *Inorg. Chem.,* 2006, **45**, 10282.
35 T. Hirano, K. Ueda, M. Mukaida, H. Nagao and T. Oi, *J. Chem. Soc., Dalton Trans.,* 2001, 2341.
36 I. Sasaki, S. Amabilino, S. Mallet-Ladeira, M. Tassé, A. Sournia-Saquet, P.G. Lacroix and I. Malfant, *New J. Chem.,* 2019, **43**, 11241.
37 D. Tsikas, *J. Chromato. B,* 2007, **851**, 51.
38 J. Liu, Q. Duan, J. Wang, Z. Song, X. Qiao and H.J. Wang, *Biomed. Opt.,* 2015, **20**, 1.
39 M.N. Patel, D.S. Gandhi, P.A. Parmar and H.N. Joshi, *J. Coord. Chem.,* 2012, **65**, 1926.
40 S.S.M. Fernandes, M. Belsley, C. Ciarrocchi, M. Licchelli and M.M.M. Raposo, *Dyes Pigm.*, 2018, **150**, 49.
41 P. Labra-Vázquez, A.Z. Lugo-Aranda, M.; Arcos-Ramos, R. Maldonado-Domínguez, M.d. P. Carreon-Castro, R. Santillan and N. Farfán, *J. Mol. Struct.,* 2015, **1101**, 116.
42 P. Labra-Vázquez, M. Palma-Contreras, R. Santillan and N. Farfán, *J. Mol. Struct.,* 2017, **1131**, 156.
43 Bruker (2005), *SADABS*, Bruker AXS Inc., Madison, Wisconsin, USA.
44 G.M. Sheldrick, *Acta Cryst*., 2015, **A71**, 3.
45 L. Palatinus and G. Chapuis, *J. Appl. Cryst.,* 2007, **40**, 786.
46 G.M. Sheldrick, *Acta Cryst.,* 2008, **A64**, 112.
47 P.W. Betteridge, J.R. Carruthers, R.I. Cooper, K. Prout and D.J. Watkin, *J. Appl. Cryst.,* 2003, **36**, 1487.
48 Gaussian 09, Revision A.02, Frisch, M. J.; Trucks, G. W.; Schlegel, H. B.; Scuseria, G. E.; Robb, M. A.; Cheeseman, J. R.; Scalmani, G.; Barone, V.; Petersson, G. A.; Nakatsuji, H.; Li, X.; Caricato, M.; Marenich, A. V.; Bloino, J.; Janesko, B. G.; Gomperts, R.; Mennucci, B.; Hratchian, H. P.; Ortiz, J. V.; Izmaylov, A. F.; Sonnenberg, J. L.; Williams-Young, D.; Ding, F.; Lipparini, F.; Egidi, F.; Goings, J.; Peng, B.; Petrone, A.; Henderson, T.; Ranasinghe, D.; Zakrzewski, V. G.; Gao, J.; Rega, N.; Zheng, G.; Liang, W.; Hada, M.; Ehara, M.; Toyota, K.; Fukuda, R.; Hasegawa, J.; Ishida, M.; Nakajima, T.; Honda, Y.; Kitao, O.; Nakai, H.; Vreven, T.; Throssell, K.; Montgomery, J. A., Jr.; Peralta, J. E.; Ogliaro, F.; Bearpark, M. J.; Heyd, J. J.; Brothers, E. N.; Kudin, K. N.; Staroverov, V. N.; Keith, T. A.; Kobayashi, R.; Normand, J.; Raghavachari, K.; Rendell, A. P.; Burant, J. C.; Iyengar, S. S.; Tomasi, J.; Cossi, M.; Millam, J. M.; Klene, M.; Adamo, C.; Cammi, R.; Ochterski, J. W.; Martin, R. L.; Morokuma, K.; Farkas, O.; Foresman, J. B.; Fox, D. J. Gaussian, Inc., Wallingford CT, 2016.
49 M.J. Rose and P.K. Mascharak, *Inorg. Chem.,* 2009, **48**, 6904-6917.
50 P. Hirva, M. Haukka, M. Jakonen and M.A. Moreno, *J. Mol. Model.,* 2008, **14**, 171-181.
51 A.W. Ehlers, M. Böhme, S. Dapprich, A. Gobbi, A. Höllwarth, V. Jonas, K.L. Köhler, R. Stegmann, A. Vedkamp and G. Frenking, *Chem. Phys. Lett.*, 1993, **208**, 111-114.
52 J. Tomasi, B. Mennucci and R. Cammi, *Chem. Rev.,* 2005, **105**, 2999.
53 D. Laurent and D. Jacquemin, *Int. J. Quant. Chem.,* 2013, **113**, 2019.
54 A.R. Allouche, *J. Comput. Chem.,* 2011, **32**, 174.
55 GABEDIT: http://gabedit.sourceforge.net/
56 V. Pimienta, C. Frouté, M.H. Deniel, D. Lavabre, R. Guglielmetti, J.C. Micheau, *J. Photochem. Photobiol. A*, 1999, **122**, 199 (ref. 35)
57 Sa3.3 software can be downloaded at http://cinet.chim.pagesperso-orange.fr/.

ARTICLE